الجمهورية الجزائرية الديمقراطية الشعبية

وزارة التعليم العالي والبحث العلمي

People's Democratic Republic of Algeria

Ministry of Higher Education and Scientific Research

Saad Dahleb Blida University 1

Faculty of sciences

Physics Department

Final Thesis

For obtaining the Master's degree in physics

Option: Nanophysics

Theme:

ENHANCED PHOTOVOLTAIC PERFORMANCES OF GRAPHENE/Si SOLAR CELLS BY INSERTION OF AN MoS_2 THIN FILM

Presented by :

Ouchene Nedjm Eddine

Hadj Abdelkader Zakaria

Jury Member:

Mr. A. BENHAFFAF	MAA, USDB1	President
Dr. H. TAHI	Dr,CDTA	Examiner
Dr. A. Hassein-Bey	MCB, USDB 1	Supervisor
Mr . A.TAHRAOUI	Doctorant, USDB1	Co-Supervisor

Blida , November, 2019

Dedication

I dedicate this humble work, with all my love and respect,

To my late **father**, Djilali, and my great **mother**, who has always believed in me,

Her compassion, patience, care and encouragement,

My brother Ali and my sisters, my wife my extended family, my childhood friends and my neighbors,

All my graduate professors, all my graduate colleagues,

My country: Algeria, its flag and its national anthem,

Zakaria

Dedication

I dedicate this humble work, with all my love and respect,

To my late **father**, Ahmed, and my great **mother**, who has always believed in me,

Her compassion, patience, care and encouragement,

My brothers and my sister, my wife, my extended family, my childhood friends and my neighbors,

All my graduate professors, all my graduate colleagues,

My country: Algeria, its flag and its national anthem,

Nejmeddine

Acknowledgements

First, we would like to thank the two persons that Allah has blessed us with in our life; ***Our Parents*** *who sacrificed their youth and energy, and gave us all their love and support to transform the lives they gave us into wonderful adventures. We are so glad and blessed to be able to wake up every day and see their smiles. We wish that we make them proud, and that they can finally pick up the fruits of their efforts.*

Secondly, we would be more than glad to thank our advisor "Dr. Ahmed Tahraoui" for all the patience, time and efforts that he was so generous to give to us during the period of accomplishing this work. Despite him being very far from his homeland, which caused some difficulties in communication, and the fact that we knew very little about Solar Energy did not prevent him from believing in us and giving us opportunity to learn and work with him. This allowed us to gain valuable knowledge, experience, confidence and a strong will to accomplish this work and try to contribute to the field of Solar Energy. We wish him all the success in all the projects that he is working on.

Above that, we would like to thank "Dr. Abdelkader Hassein-Bey" for the efforts that he put into opening the branch of Nano-physics, which allowed us to access this amazing field of "Microsystems». In addition to this, we thank him for the efforts that he put into teaching us for longer hours every day, several days a week, all of this to deliver us valuable information that we certainly found helpful in the work reported in this thesis. Furthermore, we should thank him for co-advising us and bringing valuable help by providing us with innovative solutions and encouraging us when facing problems.

We would address our acknowledgements to the members of the jury, starting with the president of the jury "Dr. H.Tahi", the examiner "Mr. A.Benhaffaf", and the advisors "Mr. A.Tahraoui" and "Dr. A.Hassein-Bey", for giving us the honor to examine this work, and for the time and efforts that they have taken to read and correct this manuscript.

We will certainly not forget all the teachers that taught us through all these academic years.

At last, it is more than a pleasure to address our acknowledgement to our family members, friends and every person that gave us material and emotional support, just to push us to study and reach this level.

Abstract

Since the discovery of graphene in 2004, this has opened a wide scope for the study of this substance with special characteristics; It also opened the way for what is known as two-dimensional materials, Particularly metallic transition decalicogridines, the most important of which is MoS_2.

In this thesis, we simulated an experiment by a group of researchers headed by “Yuka Tsuboi”, “Feijiu Wang”, “Daichi Kozawa”, based on the silvaco TCAD program. The team compared two solar cells consisting of graphene and silicon n-type and the graphene / MoS_2 / silicon n-type.

We performed this simulation under AM1.5 radiation and we got a yield of about 10% for the cell to which I added a nanometer strip of sulfur molybdate.

Résumé

Depuis la découverte du graphène en 2004, cela a ouvert un vaste champ pour l’étude de cette substance aux caractéristiques spéciales; Il a également ouvert la voie à ce que l’on appelle les matériaux bidimensionnels, notamment les décalcogridines à transition métallique, dont le plus important est le MoS_2.

Dans cette thèse, nous avons simulé une expérience menée par un groupe de chercheurs dirigé par « Yuka Tsuboi », « Feijiu Wang » et « Daichi Kozawa », sur la base du programme silvaco TCAD, L’équipe a comparé deux cellules solaires constituées de graphène et de silicium de type n et du graphène / MoS_2 / silicium de type n.

Nous avons effectué cette simulation sous rayonnement AM1.5 et nous avons obtenu un rendement d’environ 10% pour la cellule à laquelle nous avons ajouté la bande nanométrique de molybdate de soufre.

ملخص

منذ اكتشاف الجرافين في عام 2004 فتح ذلك مجال واسعا لدراسة هذه المادة ذات الخصائص المميزة كما فتح المجال في ما بعد لما يعرف بالمواد ثنائية الأبعاد وخاصة ديكاليكوجيدينات الانتقال المعدني ومن أهمها موليبدينات الكبريت MoS_2.

لقد قمنا في هذه المذكرة بإجراء محاكاة لتجربة قام بها مجموعة من الباحثين يترأسهم "يوكا تسوبوي" و"فيجو وانغ" و"دايتشي كوزاوا" وذلك باستعمال برنامج محاكاة أجهزة أشباه الموصلات SILVACO ATLAS (TCAD). حيث قام الفريق بالمقارنة بين خليتين شمسيتين تتكون الأولى من الجرافين وsilicon n-type والثانية من الجرافين /موليبدينات الكبريت silicon n-type / MoS_2.

أجرينا هذه المحاكاة تحت إشعاع AM1.5 فتحصلنا على مردود يقارب 10% بالنسبة للخلية التي أضفنا لها شريط نانومتري من موليبيدنات الكبريت.

TABLE OF CONTENTS

LIST OF FIGURES

LIST OF TABLES

I. GENERAL INTRODUCTION

With an increase in low dimensional material research, the 2D materials (atomically thin materials) have been widely and intensively studied from the viewpoints of both fundamental physics and applications.2–9

The discovery of "graphene", the first two-dimensional flat material, in which carbon atoms are arranged periodically in a honeycomb lattice, is the block for most of the allotropes of carbon except diamond and amorphous structures. Graphene has shown highly desirable properties such as high transparency, extremely high charge carrier mobility, thermodynamic stability and mechanical hardness [10].

Graphene in its primary stage of development has been a very good candidate for applications such as field-effect transistors [11], transparent electrodes [12], liquid crystal devices [13], ultra-capacitors, ultra-tough paper [14], gas molecule detection [15], Li ion battery [16], field electron emitters [17,18] and solar cells [19,20]

The high transparency accompanied with large conductivity favors graphene as a very suitable material for transparent conductive electrode for thin film solar cells. Another important aspect of graphene is its thickness dependent semiconducting property which may favor its application in forming Schottky junction with suitable metals.

Transition-metal dichalcogenides (TMDs) (MX2; M = Mo, W; X = Se, S) are among the most attractive two dimensional (2D) layered materials that can be thinned down to atomic-scale thickness.[21] Monolayer molybdenum disulfide (MoS_2), which is a typical and well-studied TMD system, is a direct bandgap semiconductor, whereas bulk MoS_2 is an indirect bandgap semiconductor. The direct-to-indirect energy gap transition occurs in MoS_2 when it changes from a monolayer to a bilayer, and the optical bandgap changes from 1.8 eV in monolayer MoS_2 to 1.2 eV in bulk MoS_2.[04,22,23] The

optical band gap associated with their energy structures has potential applications in various optical and electronic devices.

For the scope of this work, we used SILVACO ALTAS (TCAD) software to simulate two solar cells firset one is Graphene/n-si schottky junction and the second one is Graphene/MoS_2/n-Si Schottky junction. The results show a net improvement in the efficiency of the cell Graphene/MoS_2/n-Si Schottky junction is higher than the other one.

The second chapter describes the fundamentals of semiconductors and solar cells. In the third chapter, we explain in details the physical and properties of MoS_2 and Graphene materials.

In the first part of chapter four, we explain SILVACO atlas software language and show how we should deal with this software. The second part deals with the simulation results.

Finally, this work has a conclusion that presents our results.

Chapter II

BACKGROUND

II. SEMICONDUCTOR BASICS

1. INTRODUCTION

The use of **Graphene** to improve the efficiency of solar cells is investigated in this thesis. To understand how **Graphene Based Solar Cells** function, a basic understanding of semiconductor physics is required. The fundamental principles of semiconductor physics and solar cells are reviewed in this chapter.

2. SEMICONDUCTOR BASICS

Semiconductors are materials that can act either as an electrical insulator or conductor based on the conditions in which they operate. This behavior is due to the bonding properties of the individual atoms that form a bulk material and the interactions between their outer electrons. The individual atoms of semiconductors, like all other toms, have a set structure that determines how they will bond with other atoms.

2.1. Atomic Structure and Quantum Theory

An individual atom consists of positively charged protons, neutrons with no charge, and negatively charged electrons. It is held together by the attractive forces of the oppositely charged protons and electrons. The structure of an atom consists of a central nucleus composed of protons and neutrons that is orbited by a cloud of electrons. This electron cloud is made up of quantized shells that have an associated energy level. Every electron in this orbiting cloud must reside at a quantized energy level. An electron can move to a higher energy shell by absorbing energy or drop to a lower shell by releasing energy. This arrangement of electrons in the quantized shells is the most important determining factor in an atom's interactions with other atoms and, therefore, its electrical properties.

In every atom, each electron has a unique set of quantum numbers which describe its energy state in the atom. The four quantum numbers are represented by the letters n, l, m, and s. The first number n represents the shell

that the electron occupies. Higher shell levels have electrons in higher energy states than lower shell levels. The l and m numbers denote subshells that appear within each shell and each can hold two electrons of 4 opposite spin. The s number represents the spin of the electron and can either be a positive or negative value. The possible values of each of the quantum numbers are summarized in Table 2-1.

Table 2-1. All possible values of all possible quantum numbers

Quantum Number	**Possible Quantum Number Values**
N	*n*= (1, 2, 3, …, *n*) where *n*corresponds to the energy level of the outermost shell
L	*l*= (0, 1, 2, …, *n*-1)
M	*m*= (-*l*, -*l*+1, …, *l*-1, *l*)
S	*s*= (-1/2, +1/2)

2.2. Crystal Lattice

Every solid material is made up of individual atoms organized in a certain manner and can be classified as amorphous, crystalline, or polycrystalline based on their arrangement. The basic lattice structure of amorphous, crystalline, and polycrystalline materials is shown in Figure 2-1. The most abundant solids found naturally on the earth are usually amorphous, meaning their individual atoms have no ordered arrangement. Contrastingly, a crystalline material is a material that has a periodic arrangement of atoms, called a crystal lattice, which is repeated throughout the solid. Therefore, the solid appears the same when examined at the atomic level at any point. Materials that do not fall into either the amorphous or crystalline category are classified as polycrystalline. These materials are composed of different regions that each have a periodic arrangement of atoms, but the whole material is not uniform in its arrangement.

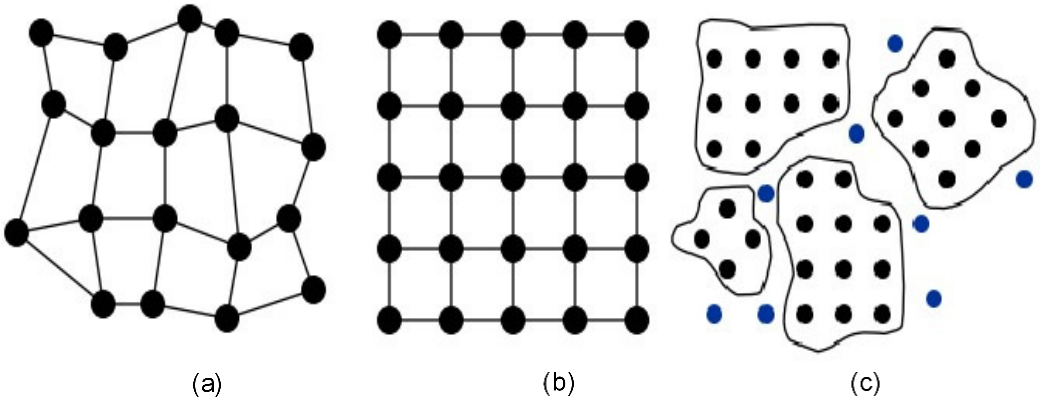

Figure 2-1 (a), 2-1(b), and 2-1(c) show the atomic structures for amorphous, crystalline, and polycrystalline materials respectively [24].

Crystalline solids, which are the most commonly used materials in solar cell applications, can be further classified based on the type of structure of their crystal lattice. Every lattice can be reduced to a unit cell, a small volume which is representative of the whole cell. This unit cell forms a geometry which can take many forms. The most common forms are the variations of the cubic and diamond lattices. An example of a diamond crystal lattice is given in Figure 2.2 A material can be thought of as a large object composed of large quantities of these unit cells put together as building blocks.

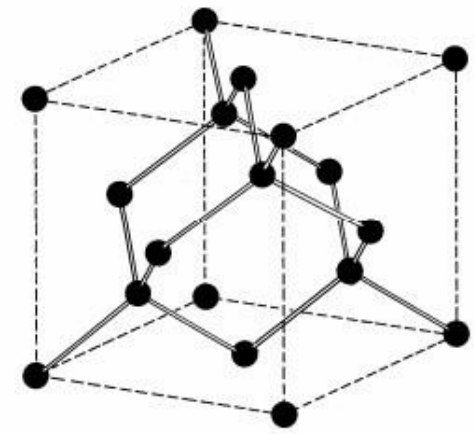

Figure 2-2: The diamond lattice is shown with each black dot representing an individual atom and each solid line representing a bond between atoms [24].

A semiconductor material's unit cell structure determines many of its important properties in solar and electrical applications. The numbers and types of bonds between atoms of the material determine the characteristics of the flow

of charge carriers in the material, defining parameters such as resistivity and conductance. The arrangement of the atoms also determines whether certain materials can be grown in layers adjacent to one another to create a certain device. If two material lattice structures do not match in a certain manner, lattice mismatch will occur, a condition in which the lattices of two adjacent materials cannot create an appropriate electrical interface due to conflicting lattice structures. These properties governed by the crystal lattice combine with the properties and structure of the individual atoms to give every material unique properties.

2.3. Energy Bands

In much the same way that electrons can only reside at certain quantized energy levels in an individual atom, they are restricted to inhabiting energy bands in a solid. However, each of these energy bands is made up of a range of energy levels that each electron can occupy. This difference arises from the influence of all neighboring atoms on an electron. In the case of an individual atom, an electron resides in a quantized shell with an associated energy level. If two atoms are close enough to each other, their electrons and other attractive forces will influence each other, creating different energy states in specific bands of energy. In the band diagram in Figure 2-3, interatomic distance is graphed against electron energy. The band diagram shows that when atoms of the same element are infinitely far away from each other, they have the same quantized energy levels. However, when the atoms are closer together, the electrons of each atom interact, and the discrete energy levels diverge into a band of allowed energies shown by the grey portion of the graph in Figure 2-3.

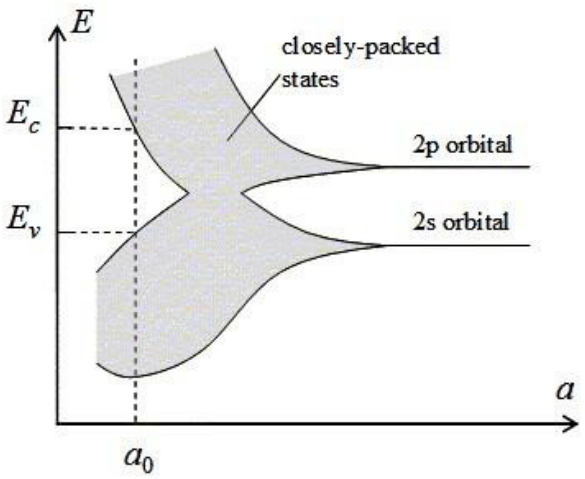

Figure 2-3: Inter-atomic distance is graphed against energy to show the formation of energy bands in a material [25].

The only energy bands of major concern in solar cell applications are the valence band and the conduction band. The valence band is the outermost energy shell of each atom. The electrons in this band are usually held in place by bonds between atoms. If an electron in the valence band receives energy greater than or equal to the difference in energy in the conduction and valence band, known as the bandgap, then it will move into the conduction band. When it moves into the conduction band, the electron breaks away from its bond and becomes a free electron in the material. An electron can only move up to the conduction when gaining energy in the valence band because there are no allowable energy states for an electron to occupy within the bandgap.

A material's ability to conduct electricity is highly dependent on its bandgap. Insulators have a relatively large bandgap and take a large amount of energy to excite free electrons. Semiconductors have a relatively small bandgap, allowing them to act as an insulating or conducting material dependent on the level of energy in the material. Conductors have overlapping valence and conduction bands and, therefore, have free charge carriers without the addition of outside energy. The differences in bandgap among insulators, semiconductors, and conductors are shown in Figure 2-4. The bandgap decreases as conduction ability increases.

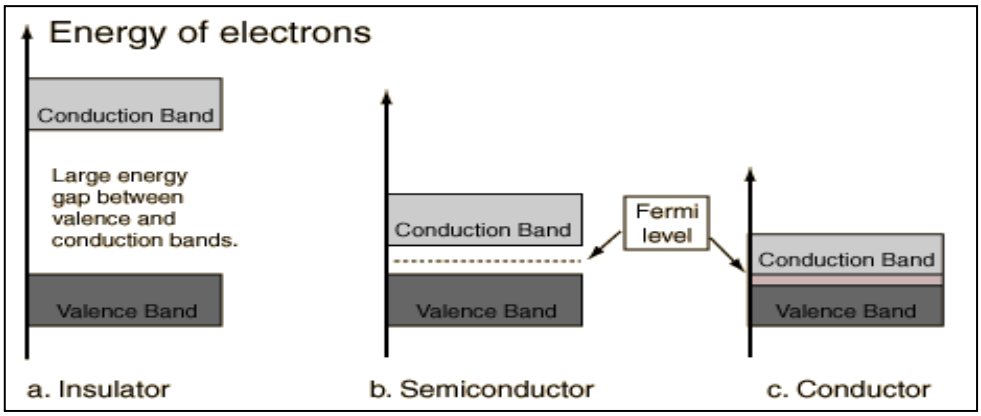

Figure 2-4: The relative bandgaps of insulators, semiconductors, and conductors are shown in Figures 4(a), 4(b), and 4(c) respectively [25].

Semiconductors have a moderate bandgap due to the unique conditions in their valence bands. All elemental or single element semiconductors have four electrons in the valence band of each atom. These elements are known as group IV elements. The atoms of these materials bond with each other to fill the outer shell of each of the surrounding atoms by the use of four covalent bonds with neighboring atoms. These covalent bonds can be broken by the introduction of energy, which frees charge carriers. Other semiconductors are made up of compounds in which the two element's valence electrons sum to eight. This can be achieved in many different elemental combinations to create effective semiconductor materials.

2.4. Charge Carries

When bonds are broken in a material due to the absorption of energy, two different types of charge carriers are created called electrons and holes. Electrons are simply the negatively charged elements of atoms and are considered free electrons when they break away from a bond. Holes are conversely the positive charge left behind by the broken bond of the free electron. Unlike free electrons, holes exist in the valence band. Holes are not physical particles but are merely positive charges created by the lack of necessary electrons for charge balance. Though holes are not physical particles with a mass, their flow is associated with a positive value of current while electron flow is associated with negative current.

Electrons and holes each have an associated mobility in every material based on how easily the free charge carriers can move through the material. Though electrons and holes are of equal charge, electrons have a higher mobility. A material's electron and hole mobility are dependent on many material characteristics such as the lattice structure, the size of the atoms in the material, and the orientation of the channel in which the charge carrier is travelling. The electron and hole mobility determine parameters such as the conductance and resistivity of a material, which are important factors in solar cells.

2.5. Doping

Doping means the introduction of impurities into a semiconductor crystal to the defined modification of conductivity. Two of the most important materials silicon can be doped with, are boron (3 valence electrons = 3-valent) and phosphorus (5 valence electrons = 5-valent). Other materials are aluminum, indium (3-valent) and arsenic, antimony (5-valent).

The dopant is integrated into the lattice structure of the semiconductor crystal, the number of outer electrons define the type of doping. Elements with 3 valence electrons are used for p-type doping, 5-valued elements for n-doping. The conductivity of a deliberately contaminated silicon crystal can be increased by a factor of 10^6.

2.6. P-N Junction

Most of the applications of semiconductors, including solar cells, are possible due to the properties created by the junction between a p-type region and an n-type region. The region where these two materials meet is called a **p-n junction** and functions as a diode. In this region, excess electrons in the n region and excess holes in the p region diffuse across the border of the two regions to form a depletion region in which oppositely charged ions create a barrier that blocks charge flow. The formation of the depletion region from the junction of p-type and n-type materials is shown in Figure 2-5.

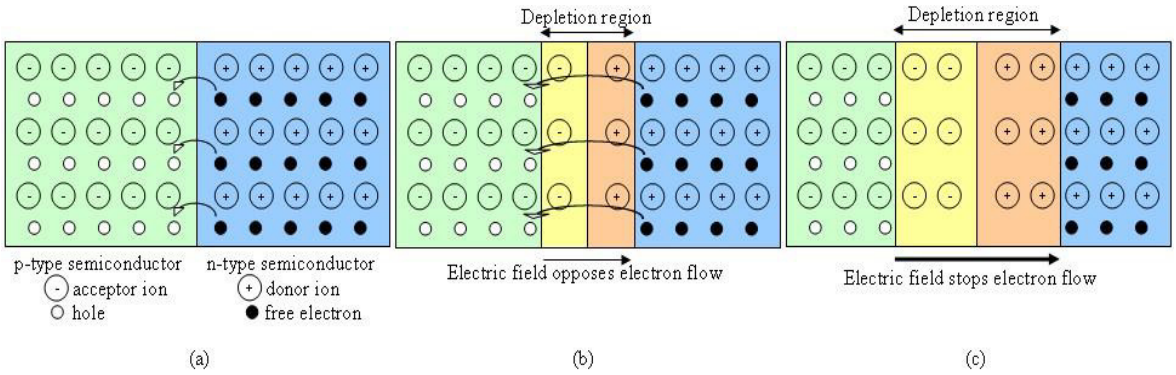

Figure 2-5: The junction between an n-doped and p-doped material forms a depletion region. (a) Shows majority carriers travelling across the junction due to the attraction caused by opposite charge carriers. The barrier caused by newly formed ions is shown in (b) and (c) [26].

The instant the materials meet, the excess carriers of each material border region move to the other side, attracted by the holes or electrons on the other side of the junction. These charges leave behind ions that then have a negative charge in the case of the p side and a positive charge in the case of the n side. This barrier then blocks charge flow because the electrons on the n side are repelled by the negative region on the edge of the n side and the opposite is true of the holes on the p side. If the junction is forward biased with a voltage greater than the potential of the depletion region potential, then the diode conducts current. If the diode is reversed biased, it acts as an insulator and the depletion region expands.

2.7. Metal/Semi-Conductor (Schottky) Junction

The point contact diode is one of the earliest solid-state semiconductor devices constructed. This type of diode is made bymaking contact between a Metal a Semiconductorsurface. The point contact diode was later studied by Walter H. Schottky circa 1938 who formulated a theory as to why the diode worked; subsequently this device was named the Schottky diode to honor his contributions. Due to the fabrication simplicity of this device, the Schottky diode makes an excellent choice for testing experimental processes in semiconductor manufacturing.

This structure is the basis of a large number of some electronic structures that are more complex than the conventional ones.

The semiconductor material for this study will be *Molybdenum disulfide* (**MOS_2**) with n-type doping. The material that will mimic the metal that composes the other half of this device (conductor) will be Graphene, which always has a large abundance of free electron charge carriers.

All metals have a *work function* $\boldsymbol{\phi_m}$: the energy it takes to remove an electron from the atom to the vacuum level potential. The attributes of both metal and semiconductor while separated are illustrated in Figure 2-6. The potential energy needed to inject charge carriers from the metal into the semiconductor material is the *Schottky Barrier Height* measured in *electron volts* (**eV**). The Schottky Barrier Height value is the energy it takes to remove an electron from the metal minus the energy required to detach an electron from the n-type semiconductor material, which is the *electron affinity* χ creating electron flow from the semiconductor to the metal. The Schottky Barrier Height can be calculated for a Schottky diode by the following equation:

$$\phi_B = \phi_m - \chi \tag{2.1}$$

The Schottky Barrier Height (often referred to as **SBH**) is a fixed amount of energy drop across the diode, this value is unique to the combination of metal and semiconductor, ideally this does not vary with forward voltage biasing or current flow. However, the phenomenon of *SBH lowering* may occur in reverse bias due to electric field crowding [27].

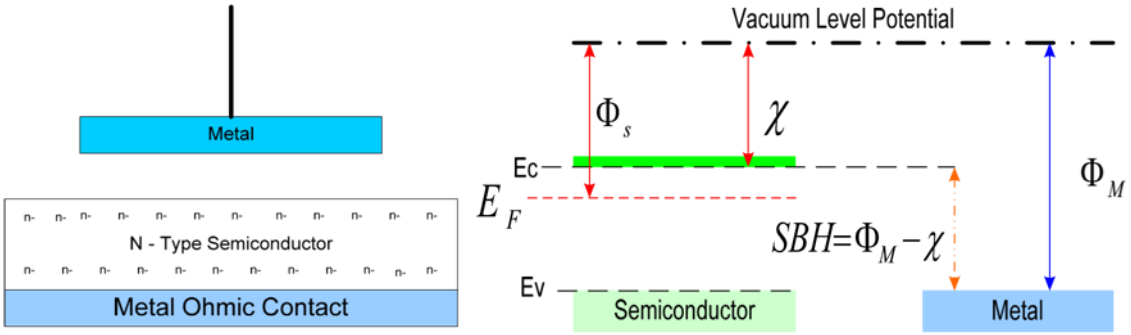

Figure 2-6: Metal and semiconductor before contact; band diagram Schottky barrier height.

When the metal contacts the semiconductor, there is an imbalance of Fermi energy states in the two materials and the charges migrate to reach equilibrium levels. To simplify this matter, some of the electrons in the n-type semiconductor migrate into the metal leaving behind a region of material with no free charge carriers. This area is called the depletion region, and the energy it takes to cross this region is known as the built-in potential. This concept is illustrated in Figure 2-7.

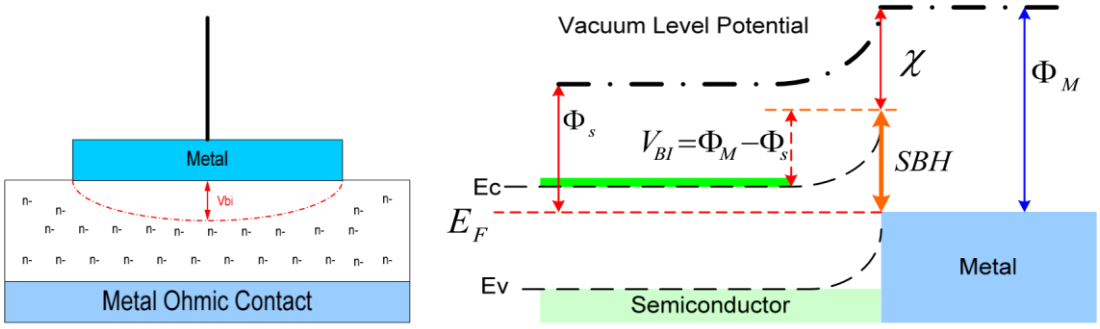

Figure 2-7: Metal and semiconductor in contact; band diagram of built-in potential.

The built-in potential V_{BI}also referred to as "*equilibrium contact potential*" (occurring when the Fermi levels have reached a balance) is the mechanism that prevents any further charge movement from the semiconductor conduction band to the metal. This built-in potential V_{BI} is the difference in the work function of the metal and the work function of the semiconductor.

$$V_{BI} = \phi_m - \phi_s \tag{2.2}$$

The built-in potential V_{BI}, the applied voltage, and the doping concentration play a large role in the width of the depletion region. This depletion region is absent of charge carriers in the semiconductor essentially behaving as a layer of insulation. The width$W$ of this depletion region is related to both the built-in potential and doping concentration. Where V_a is the applied biasing voltage with $N_a$and $N_d$being the acceptor/donor carrier concentrations, it is theorized that electrons (donors) in the n-material migrate into the metal and have a mirrored electric positive (acceptor) potential in the semiconductor opposite the depletion

region. So that N_a = $N_d$and the equation of 2.3 for p-n junctions may be used to model the Schottky diode [05].

$$W = \sqrt{\frac{2\varepsilon.(V_{BI}-V_a)}{q}.\left(\frac{N_a+N_d}{N_a.N_d}\right)} \tag{2.3}$$

The below illustration of Figure 2-8 helps to show why the doping concentration N_a may be considered equal to N_d because of the mirrored electric field in the metal [27]. This depletion width can be manipulated by applying voltage across the device, which will allow for passage ofor resistance to the flow of electricity. When a forward biasing voltage V_a is applied to the Schottky diode the work function of the semiconductor material ϕs is reduced and thus the built-in potential is lowered as well.

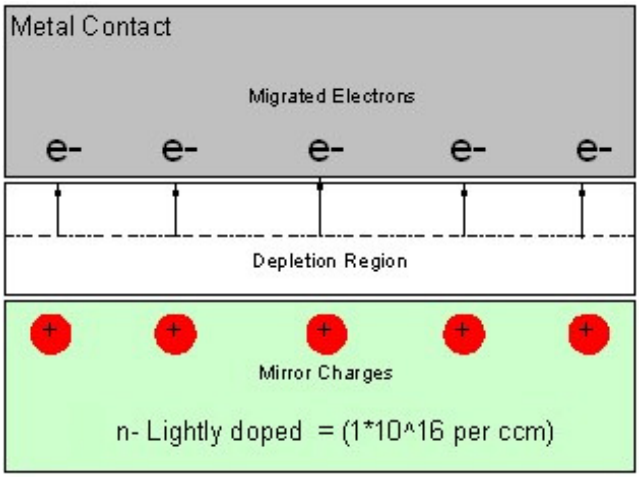

Figure 2-8: Mirrored electric dipole potentials of the Schottky contact depletion region.

The exponential current through the diode can be modeled by equation (2.4) below.

$$I_F = I_0\left(e^{\frac{qV_a}{kT}} - 1\right) \tag{2.4}$$

The forward current I_F through the diode depends exponentially on the applied voltage V_a. The initial current I_0 forms in the depletion region with both with currents both equal and opposite in equilibrium conditions, thus it can be factored out [28].

Figure 2-9 shows an illustration of the conducting diode and the accompanying energy band diagram. During forward bias with the depletion region reduced and the electrons migrating over the Schottky barrier and moving from the n-type semiconductor material to the metal contact. From the energy band diagram, the Fermi level of the semiconductor is raised by the value of the applied voltage. It should be noted that the metal at the bottom of the semiconductor has been prepared to be ohmic having a linear current voltage relationship and possess a very low value of resistance that does not play a role in the ideal analysis of the Schottky diode current [27].

During the reverse bias mode of the Schottky contact the applied voltage reinforces the built-in potential and creates a wider depletion region within the material. Because of the large negative value, the applied voltage the forward current term tends to zero leaving just the reverse initial current that no longer has an opposing forward bias equilibrium current.

$$I_R = -I_0 \tag{2.5}$$

The initial current I_0 of the device under thermal equilibrium can be approximated by knowing the SBH of the diode given equation 2.1 along with the charge of the electron and the thermal voltage [27].

$$I_0 \propto e^{\frac{-q\phi_B}{kT}} \tag{2.6}$$

During reverse bias with the depletion region widens and the only electrons that migrateover the Schottky barrier, those that existed in thermal equilibrium of the initial currentI_0. Figure 2-10 shows a reverse bias diode illustration and the band diagram of the Fermilevel of the semiconductor lowered by the value of the applied voltage.

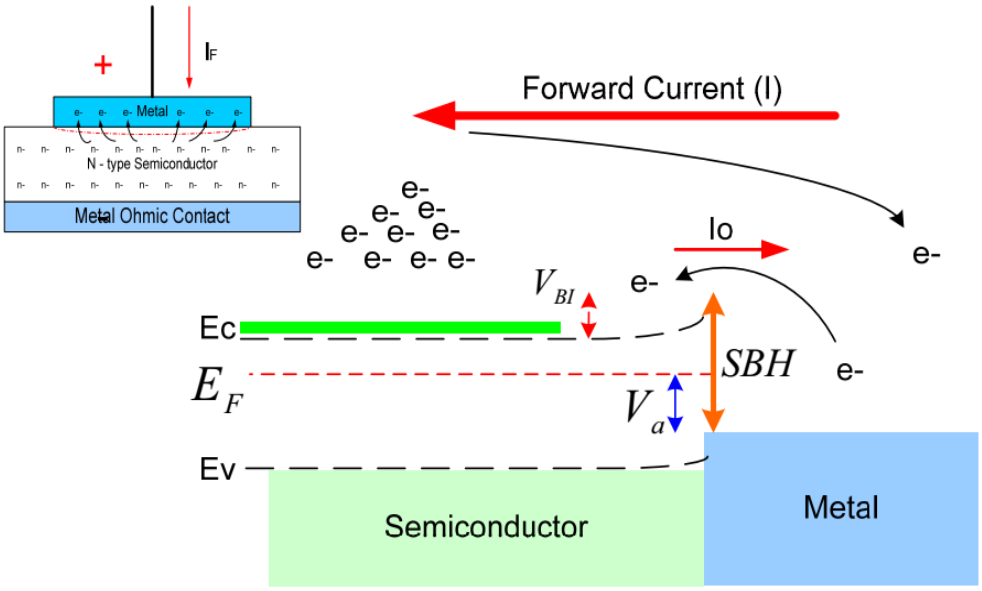

Figure 2-9: Schottky diode with energy band diagram showing the forward flow of electrical current through the diode.

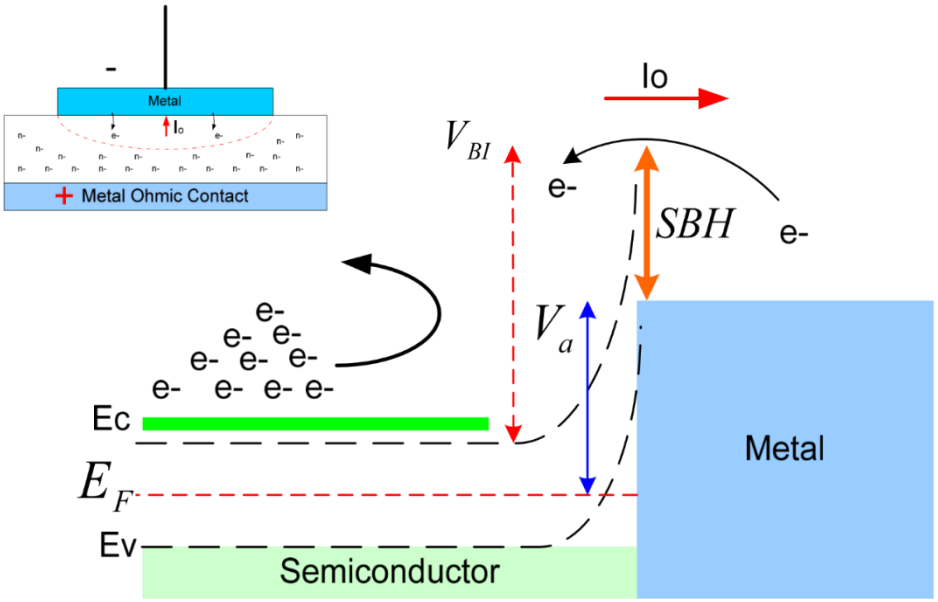

Figure 2-10: Schottky diode with energy band diagram showing the reverse bias V_a applied to the diode that increases the built-in potential.

Aspects that affect the magnitude of current through the ideal Schottky diode are the area (A) of the metal contacting the semiconductor, the temperature (T) of the material, and the Richardson's constant (A*) for the material which is a relation of current density and temperature. With these values known for the material, a more accurate and comprehensive formula for the Schottky diode contact current may be expressed by equation 2.7. This equation also accommodates deviation from ideal diode performance by a factor of *n*. This value is known as the ideality factor and for the ideal diode; this value should be nearly equal to one.

$$I_F = A.A^*.T^2 e^{\frac{-q\phi_B}{kT}}\left(e^{\frac{qV_a}{nkT}} - 1\right) \tag{2.7}$$

Now that a more accurate expression to describe the Schottky diode has been composed,it is necessary to discuss some of the aspects of the non-ideal Schottky diode. Various aspects of the material and fabrication will cause considerable deviation from the diode performance predicted by equation 2.7. Some of the ways in which variation from the ideal diode characteristics can occur are offset potentials and linearization due to resistance. While in the reverse direction carrier generation can cause a steadily increase current greater than that of I_o and conduction of electrical current in reverse bias will occur due to Zener and avalanche breakdown [28].

Current linearization due to on resistance could be the cause of a poor quality ohmic contact or a poor quality Schottky contact interface. Both of these will contribute to a high series resistance within the diode. When large currents and voltages are applied to the diode the otherwise exponential I-V curve will become linear. At this point the linear part of the I-V curve may be evaluated with the help of equation 2.8 and the value for the total series resistance of the diode may be calculated by finding the change in voltage over the change in current [28].

$$R_S = \frac{\Delta V}{\Delta I} \tag{2.8}$$

In the reverse bias operation of a Schottky diode there are several mechanisms that create current flow through when the diode should be in a

high resistance mode due the applied reverse polarity. Carrier generation in a neutral transition region occurs due to thermal activity and the nature of the semiconductor in regard to what carrier generation - recombination centers may be in the material. A significant aspect of the diode is the reverse breakdown voltage that occurs when the diode in the reverse bias mode begins to conduct electrical current exponentially. There are generally two mechanisms that contribute to reverse bias breakdown. These phenomena are known as avalanche multiplication and quantum mechanical tunneling. Neither of these two breakdown methods will destroy the diode, however heating of the diode could occur due to the high currents due to voltage breakdown which could result in permanent device failure [30]. Avalanche breakdown is created by impact ionization occurring when a large electrical potential is applied across the device and high energy electrons cross the barrier and trigger other electron hole pairs to form. *Zener* breakdown is attributed to a mechanism known as quantum mechanical tunneling which effectively allows the charge to penetrate the barrier of forbidden region. The applied reverse voltage at which these mechanisms of breakdown will occur can be estimated by the following equation of 2.9 that relates the breakdown electric field for the material E_c with the doping concentration N_d [28].

$$V_{RB} = \frac{\varepsilon_0 \varepsilon_m (E_c)^2}{2qN_d} \tag{2.9}$$

The best way to reduce currents resulting from the preceding phenomenon is to reduce the field intensity across the device. One of the most influential aspects to electric field intensity surrounding a Schottky contact is the physical shape of the metal in contact with the semiconductor forming the diode junction. Many techniques for design and construction of Schottky diode contacts implement varied contact geometries so that reverse breakdown voltages may be increased.

3. SOLAR CELL OPERATION

Due to the properties of the p-n junction and the ability of semiconductors to absorb energy via photons of light, solar cells are able to generate power.

The basic concepts behind solar power and the important characteristics that can quantify a solar cells performance are explained in this section.

3.1. Origin of Solar Power

A basic solar cell consists of a p-n junction with metal contacts on both sides of the junction. In an n on p solar cell the top n layer is called the emitter, while the bottom p side is called the base. When placed in an environment with light, the solar cell absorbs photons, which generate electron hole pairs near the depletion region. To generate power, the metal contacts to the emitter and base are tied together via an external load as shown in Figure 2-11. Due to the field of the depletion region, charge carries generated by photons are swept across the depletion region so that a photocurrent is generated in the reverse biased direction. However, when an external load is applied, the current induces a voltage across the load. This voltage induces a countering forward biased current that is less than the photocurrent but increases as the load reaches infinity. The net current in a solar cell is always in the reverse biased direction but decreases as the forward biased current increases with an increasing load. The power produced by the cell is the product of the net current and voltage across the load.

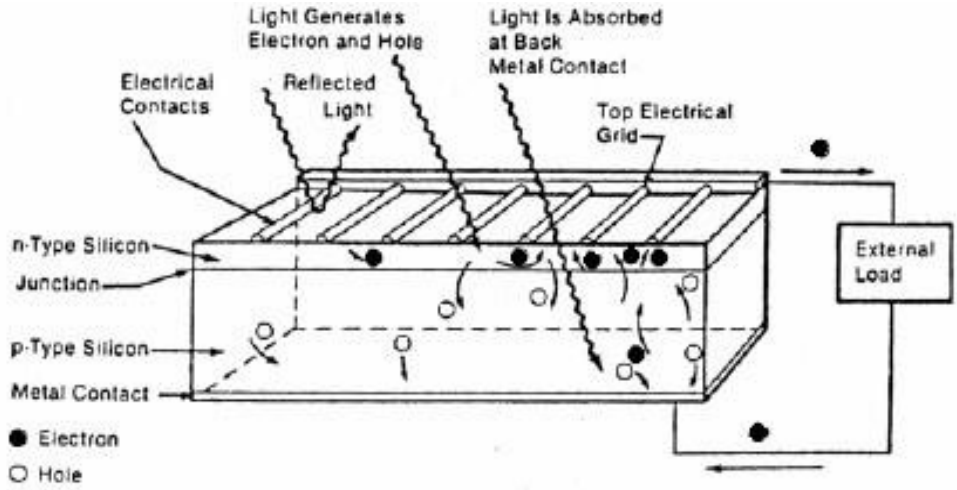

Figure 2-11: Power is delivered to an external load from a simple n on p solar cell (arrows denote electron flow) [29].

3.2. Solar Cell Characteristics

The most useful characteristic of a solar cell is its current-voltage (I-V) curve. This curve graphs the solar cell's net current per unit surface area in the y direction, against the associated load voltage in the x direction. A typical solar cell I-V curve is shown in Figure 2-12, which shows anode voltage plotted against cathode current. As discussed in the previous section, the value of load resistance affects both the load voltage and net current generated in the solar cell. The y intercept of the I-V curve is the limiting case in which there is no load resistance and a maximum value of current called the short circuit current (I_{sc}) occurs. In this case there is no induced voltage across the load, creating no forward biased current to counter the photon induced current. The x intercept represents the extreme case in which the load resistance is infinite, producing a maximum voltage known as the open circuit voltage (V_{oc}). In this case no current can flow due to the infinite resistance. Opposing charges are built up on both sides of the depletion region of the p-n junction, resulting in a maximum voltage across the infinite load. Though it is useful to know I_{sc} and V_{oc} for a solar cell, it is more useful to know the maximum power point (P_{max}). The maximum power current (I_{max}) and voltage (V_{max}) can then be determined. These values show the actual power capability of a solar cell, the most important factor in the cell's application. The parameters V_{oc}, I_{sc}, Imax, and V_{max} are shown in Figure 2-12 on an I-V curve.

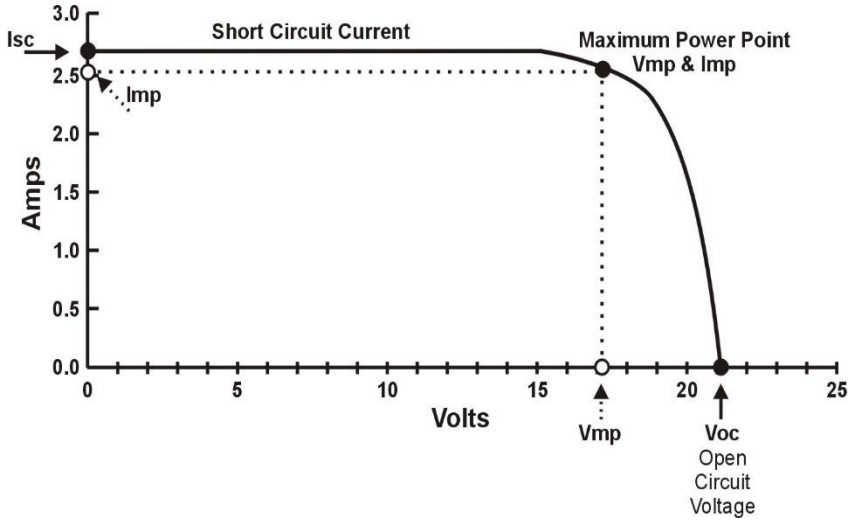

Figure 2-12: The typical I-V curve for a solar cell that graphs anode voltage against cathode current. V_{oc}, I_{sc}, I_{max}, and V_{max} are shown to display the limiting cases of the I-V curve and the maximum power point [30].

Once the I-V curve for a solar cell is determined, many parameters can be calculated which are useful in comparing the performance of different cells. Solar cell efficiency η is given by

$$\eta = \frac{P_{max}}{P_{in}} \times 100\% \tag{2.10}$$

where P_{max} is the maximum achievable power of the solar cell and Pin is the input power from the light applied to the cell. The fill factor FF is given by

$$FF = \frac{P_{max}}{I_{sc}V_{oc}} \tag{2.11}$$

where V_{oc} and I_{sc} are the open circuit voltage and short circuit current, respectively. The FF is a measure of how well a solar cell transfers its short circuit current and open circuit voltage properties into actual power. These two parameters are useful for comparing solar cells but are dependent upon the input power to the solar cell, which varies based upon the light source applied.

3.3. Solar Cell Input Power

The input power to a solar cell is dependent upon the light source in which the cell is operating. In this thesis, air mass 1.5 (**AM1.5**) is used. Solar panels do not generally operate under exactly one atmosphere's thickness: if the sun is at an angle to the Earth's surface the effective thickness will be greater. Many of

the world's major population centres, and hence solar installations and industry, across Europe, China, Japan, the United States of America and elsewhere (including northern India, southern Africa and Australia) lie in temperate latitudes. An AM number representing the spectrum at mid-latitudes is therefore much more common. "AM1.5", 1.5 atmosphere thickness, corresponds to a solar zenith angle of z=48.2°. While the summertime AM number for mid-latitudes during the middle parts of the day is less than 1.5, higher figures apply in the morning and evening and at other times of the year. Therefore, AM1.5 is useful to represent the overall yearly average for mid-latitudes. The specific value of 1.5 has been selected in the 1970s for standardization purposes, based on an analysis of solar irradiance data in the conterminous United States. [30] Since then, the solar industry has been using AM1.5 for all standardized testing or rating of terrestrial solar cells or modules, including those used in concentrating systems. The latest AM1.5 standards pertaining to photovoltaic applications are the ASTM G-173[32,33] and IEC 60904, all derived from simulations obtained with the SMARTS code.

Figure 2-13 shows the corresponding spectral irradiance for AM1.5 light beam compared with AM0 (full spectrum) spectral irradiance light beam.

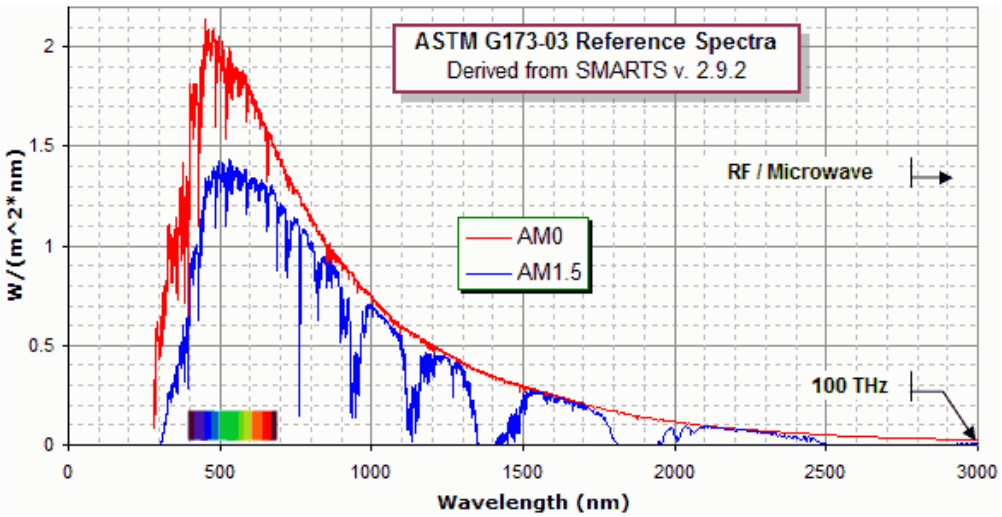

Figure 2-13: Spectral irradiance of the AM0g and AM1.5g spectrums [34].

Due to the properties of solar cells, only part of the solar spectrum can be converted into electrical power. This is caused by the different bandgaps and optical properties of materials. The bandgap of a material determines the

minimum amount of energy required to generate an electron hole pair in the material. Any photon with energy less than the bandgap will simply pass through the material without exciting an electron. The energy of a photon is dependent on its wavelength and is given by

$$E = \frac{1.24}{\lambda} \tag{2.12}$$

where *E* is in units of *eV* and *λ* is the wavelength of the photon in *μm*. The shorter the wavelength of a photon, the higher its energy and ability to generate electron hole pairs in higher band gap materials.

3.4. Solar Cell Performance

Though solar cell performance is largely dominated by a material's spectral response and I-V characteristics, there are many other factors that influence a solar cell's performance. The more important factors that affect solar cell performance are:

- The reflection of light off the surface of a solar cell limits the amount of input power into the cell. The optical properties of different materials cause a portion of the photons hitting the solar cell to be reflected off the surface. This can cause a 35% loss in the theoretical efficiency of a solar cell without the use of antireflective techniques [30].
- Photons with energy much higher than the band gap generate electron hole pairs, but the excess energy is dissipated as heat in the crystal lattice of the solar cell. Low energy photons that do not generate charge carriers also bombard the atoms in the crystal lattice and create heat. This heating causes a loss in the voltage of a solar cell. A solar cell loses 2mV/K in voltage, which can drastically lower the efficiency of a solar cell [30].
- Recombination of electrons and holes can cause the charge carriers generated by photons to meet in the lattice and cancel each other out. When this happens, a free electron meets with a hole in the valence band and occupies that space, no longer contributing to the number of charge carriers in the solar cell [30].

- Material defects in the solar cell can create traps which create more recombination. Cheaper, less pure materials can have significant defects that negate much of the generated current [30].
- The resistance of the bulk material causes a voltage drop within the solar cell that reduces the efficiency. When charge carriers are generated, they have to travel to the contacts of the solar cell to be harnessed as energy. The distance travelled through the lattice is often relatively great for each charge carrier, creating a high resistance seen by each of the charge carriers. This decreases the net voltage seen at the contacts [30].
- Shading from the top electrical contact completely blocks light to portions of the solar cell. The optimal top contact grid usually covers 8% of a solar cell. This 8% of the solar cell surface receives no photons to generate charge carriers and does not contribute to the power production of the solar cell [29].

The problems of internal resistance and shading in solar cells are addressed in this thesis through the use of Graphene. With a net reduction in the resistance seen by each of the charge carriers and a reduction in the percentage of the solar cell surface covered by the top contact, the efficiency of any solar cell can be increased. The improved conductivity on the surface of a solar cell that could be provided by a Graphene layer could be used as an electrode which collect current. These lines could, therefore, be made thicker, reducing losses from resistance in the grid lines, further increasing the efficiency of a solar cell.

4. CHAPTER SUMMARY

The background in semiconductor physics and solar cells necessary to understand the research in this thesis was provided in this chapter. The basic properties of semiconductors the theory and operations of the Schottky junction were shown to be optimal for generating solar power. The ability to generate electron hole pairs by the absorption of photons with energy greater than the bandgap allows solar cells to deliver power to a load. The producible power was shown to be dependent on both the material of the solar cell and the spectrum

of input light. The power was also shown to be limited by factors inherent in the real properties of fabricated solar cells.

The structure and properties of Graphene is covered in the next chapter to provide the basic knowledge necessary in understanding photovoltaic Graphene applications.

Chapter III

Graphene and MX_2 (MoS_2, WS_2) PROPERTIES

III. GRAPHENE AND MX_2 (MoS_2 , WS_2) PROPERTIES

III.I MX_2 (MoS_2 , WS_2) PROPERTIES

1. INTRODUCTION

The lamellar dichalcogenides constitute about two thirds of the MX2 transition metal dichalcogenides listed in the literature. In the 1970s and 1980s, they gave rise to numerous studies conducted in the laboratory under the direction of Prof. Jean Rouxel.

These compounds have a strong anisotropy of bonds: strong bonds within the layers and weaker interactions, the van der Waals interactions, ensuring the link between these layers. One of the direct consequences of such a structural organization is the possibility of making cleavages, obtaining lubricating properties or observing anisotropic physical properties. One of the most interesting points in the family of lamellar chalcogenides lies in the possibility of interposing various types of ions, or even more or less complex molecules, between the layers.

Molybdenum and tungsten disulfides and their diselenides are part of this large family of lamellar chalcogenides that adopt two-dimensional (2D) crystallographic structures.

The objective of this chapter is the study of the electronic and structural properties of WS_2 and MoS_2 lamellar compounds. The electrical and optical properties of lamellar compounds are reviewed for use in thin-film photovoltaics.

2. LAMELLAR SOLIDS

Lamellar solids are materials consisting of two-dimensional sheets stacked in the same direction; the nature of the interaxillary bonds is covalent whereas the inter-leaflet bonds are of weak interaction (Van der Waals type).

We distinguish three families of lamellar solids which differ in the constitution of their leaflets (Figure 3.1):

- atomic sheets

- molecular leaflets
- multiple leaflets

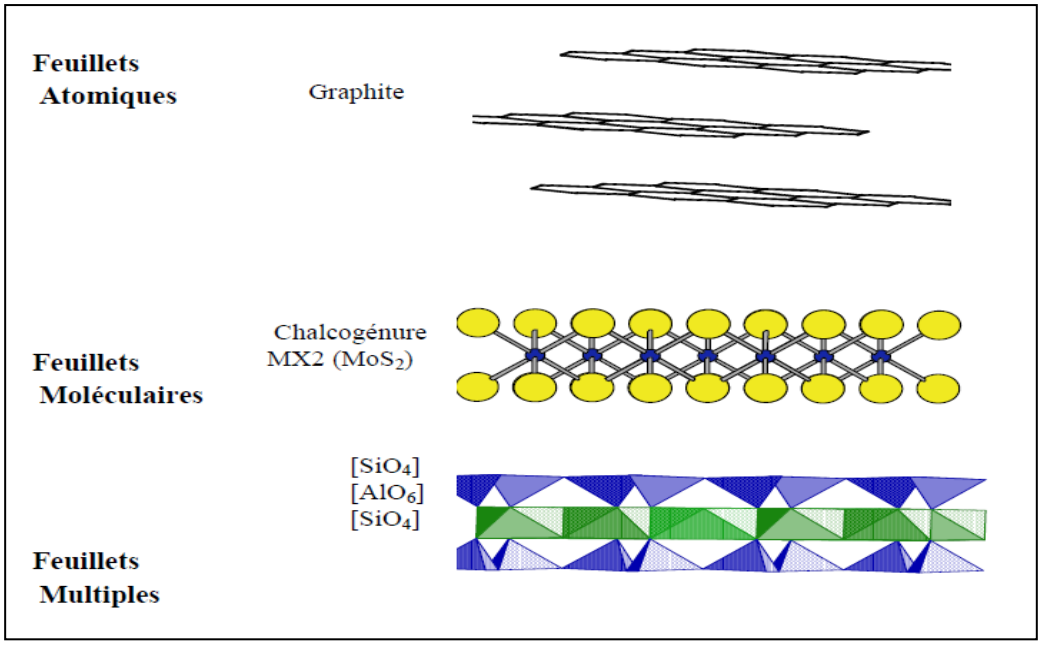

Figure 3-1: Représentatio schématique des trios familles des solides lamellaires [50].

3. TRANSITION METAL CHALCOGENIDES MX_2 (M = Ta, Nb, Ti, Re, W, Mo; X= S, Se, Te)

They are chemical compounds formed of two simple chemical elements M is a transition metal and X is a chalcogenide.

In our work we chose molybdenum and tungsten as transition metals knowing that, molybdenum is a chemical element, of symbol Mo and atomic number 42, with two electronic configurations of which one is unstable: 4d5 5s1 and the other stable: 4d45s15p 1 which gives rise to a state of hybridization sp, and the twelfth metal is tungsten which is a chemical element of the periodic table of symbol W and atomic number 74, it is a gray-white steel transition metal, very hard, and heavy, their electronic configuration is 4f14 5d4 6s2.

Sulfur has also been chosen as chalcogenides, knowing that sulfur is a chemical element of yellow color, of symbol S and of atomic number 16, its electronic configuration 3s2 3p4.

3.1. Transition metal dichalcogenides MX2 in massive form

MoS_2 transition metal dichalcogenides (TMDCs) and WS_2 are found in nature as minerals [44] [33] called molybdenite and tungstenite (wolframite).

Figure 3-2: Photographs of MoS_2 (Molybdenite) Massif [34-35]

4. THE STRUCTURAL PROPERTIES OF MX2 (M = W, Mo, X = S)

The Layred Transition Metal Dichalcoginides, TMDC which are the object of our study, have a general formula MX2 (where M = W, Mo; X = S) they contain a transition element Group VI B metal M (Mo, W) in the +4 oxidation state and two elements of the chalcogen column (S) in the oxidation state -2. Their lamellar structure results from a stack of C-axis infinite two-dimensional sheets, comprising three atomic layers according to the XMX XMX sequence. The outer layers of each sheet consist of chalcogen atoms (S) in a compact hexagonal arrangement. and in prismatic trigonal coordination with respect to metal atoms. While the central layer is composed of metal atom (Mo, W) Figure 3.3.

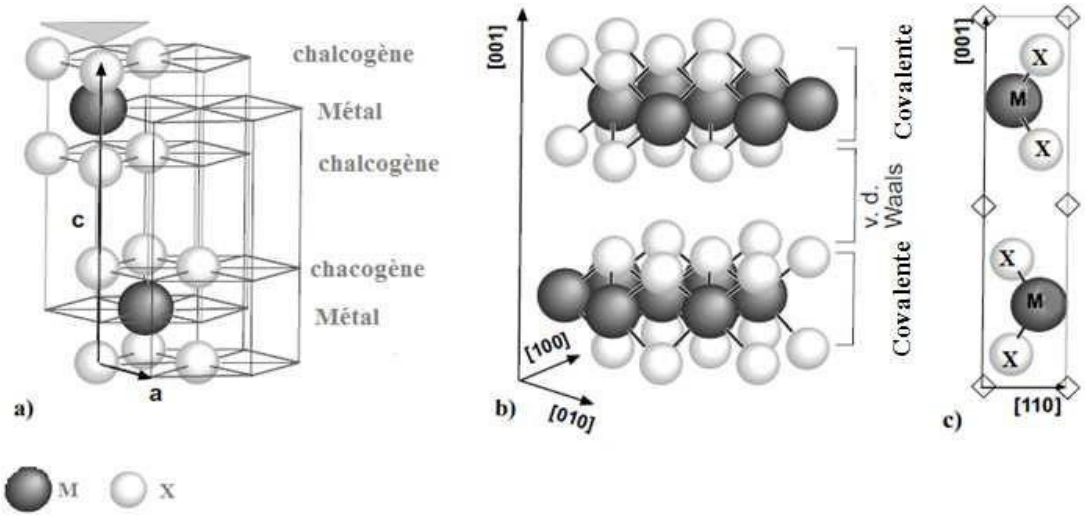

Figure 3-3: The crystal structure of MX2 [36]

The M-X bonds within the sheets are strong, of covalent nature and the inter-leaflet bonds (X-X) are much weaker van der Waals (VdW) weak. These forces are small enough to allow neighboring layers to slide through the other layers (Figure 3.4).

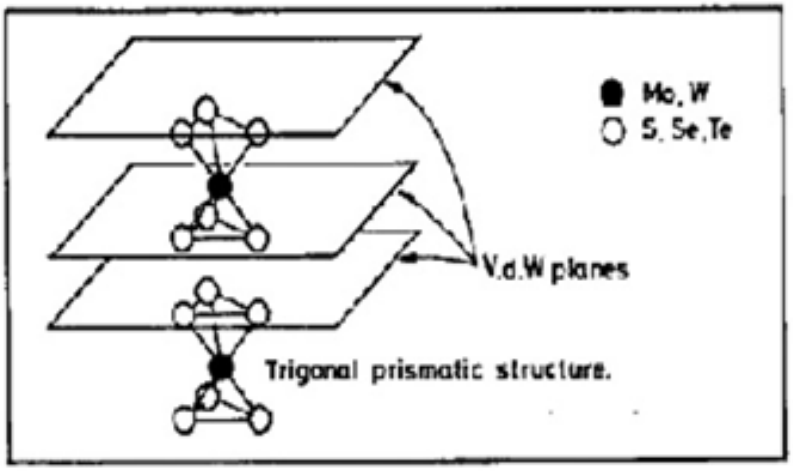

Figure 3-4: The prismatic trigonal structure of MX2 and van der Waal plans [37].

The leaflets can be stacked in two ways that result in the existence of two polytypes called 2H and 3R.

- **The polytype 2H**

In the polytype 2H, the upper sheet is rotated by 60 ° with respect to the preceding sheet, the anions and cations of the upper sheet being placed

respectively above the cations and anions of the previous sheet (Figure 3.5). There is in this case periodicity of the structure along the axis c every two sheets. The 2H-MX2 (example MoS_2) has a hexagonal symmetry with two leaflets along the c axis and the space group is D4 6h (P63 / mmc).

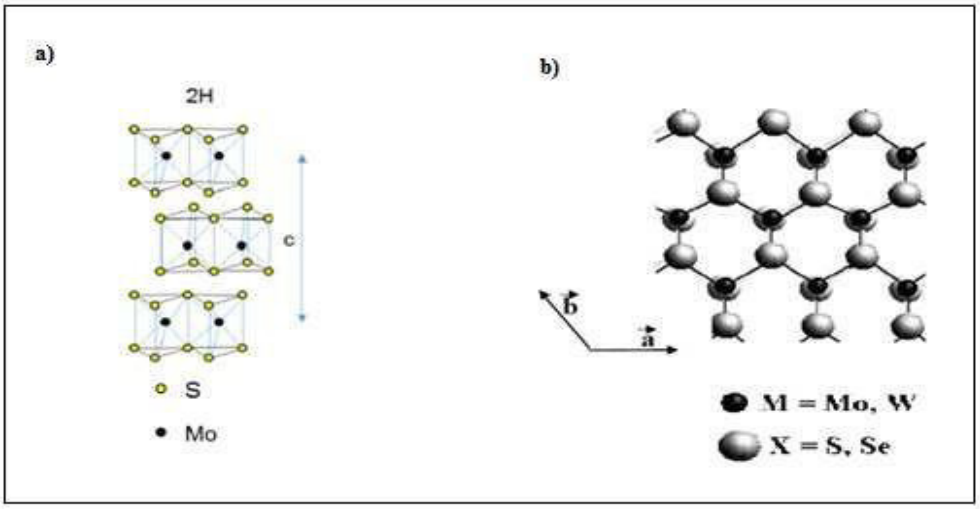

Figure 3-5: a) The 2H-MoS_2 structure along the c axis [38].

b) Projection according to [001] of two sheets of polytype 2H. [33]

- **The Polytype 3R**

In the polytype 3R, of rhombohedral symmetry C53v (R3m), each sheet retains the same orientation as the previous one but is translated in the [2,1,0] direction of 1/3 of the lattice constant. The anions are placed in this case above the interstices of the previous sheet and the cations above the chalcogenes. It takes three sheets to obtain the periodicity along the axis c (Figure 3.6).

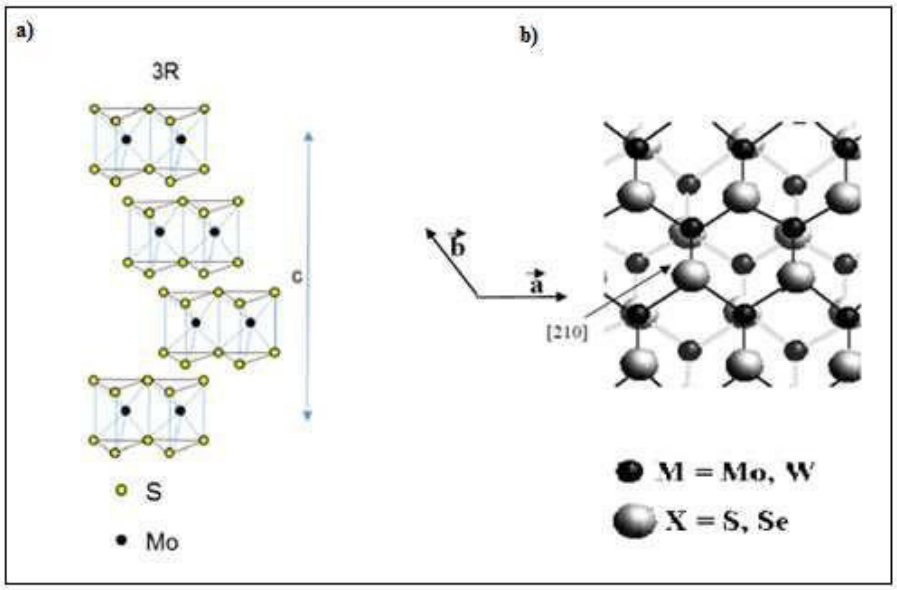

Figure 3-6: a) the 3R structure for MoS_2 along the c axis. [38]
b) Projection according to [001] of two sheets
of polytype 3R. [33]

The repeat distance of the sheets along the c axis is similar for both polytypes, for MoS_2 it is 0.615 nm. In the (002) planes, the interatomic distances X-X are equal to the lattice constants and are equal to a = b = 0.315 nm. According to the c axis, the lattice constant is 1.23 nm for the 2H polytype and 18.45 nm for the 3R polytype.

The mesh parameters of the compounds for each structure are listed in the table.3.1 below:

Table 3.1: Mesh parameters of the two compounds studied for each known polytype, frome (39):

Compound	polytype	Parameter at (A °)	Parameter c (A °)	Interleave distance, vdw plans (A °)	Density (g / cm3)
MoS_2	2H	3.160	12.294	6.147	4.96
	3R	3.163	18.37	6.123	5.02
WS_2	2H	3 .155	12.35	6.175	7.5
	3R	3.162	18.35	6.117	

5. THE OPTICAL PROPERTIES OF MX_2 (M = W, Mo, X = S)

5.1 The band structure

The transition metal dichalcogenides are diamagnetic semiconductors, the electronic structure of these compounds indicates that the top of the valence band (VBM) corresponds to the dz2 states of the metal Mo or W (partially hybridized to the p (px, py) states of the chalcogen S) and the minimum of the conduction band (CBM) being related to the dxy and dx2-y2 states thereof. (Figure 3-7).

Many optical measurements have been made on these materials and it appears that two electronic gaps exist: the first is indirect, the second is direct.

The properties of the TMDCs semiconductor electronic band structure depend on the number of layers along the C axis in the crystal, knowing that for a multilayered TMDC material there is an indirect gap band at point Γ of the zone of brillouin and for a thickness reduced to a single layer (monolayer) we will have a transition of gap from indirect to direct at the point K of the zone of brillinus see figure (3.8), this transition of gap is due to the quantum confinement effect.

The gap changes with the change of the crystal film thickness according to the equation:

$$\Delta E_g = \frac{h^2\pi^2}{2ma^2}$$ (Eq……3.1) [38] where a is the film thickness

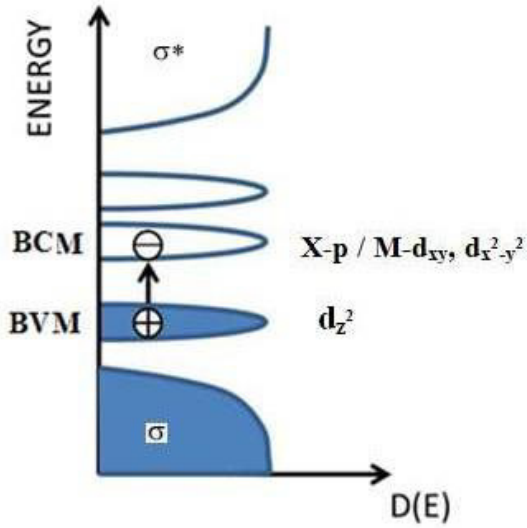

Figure 3-7: The electronic band structure of transition metal dichacogenides MX2 (M = W, Mo, X = S). [40-41]

The direct excitonic transitions at point K remain relatively unchanged with the change in layer number, which is due to the effect of quantum confinement as well as to the resulting change in hybridization between Pz orbitals on S atoms and orbitals However, the states near the point Γ are due to combinations of the Pz orbitals of the S atoms and the orbitals d of the Mo atoms and the transition at the point Γ is translated significantly from indirect to direct.

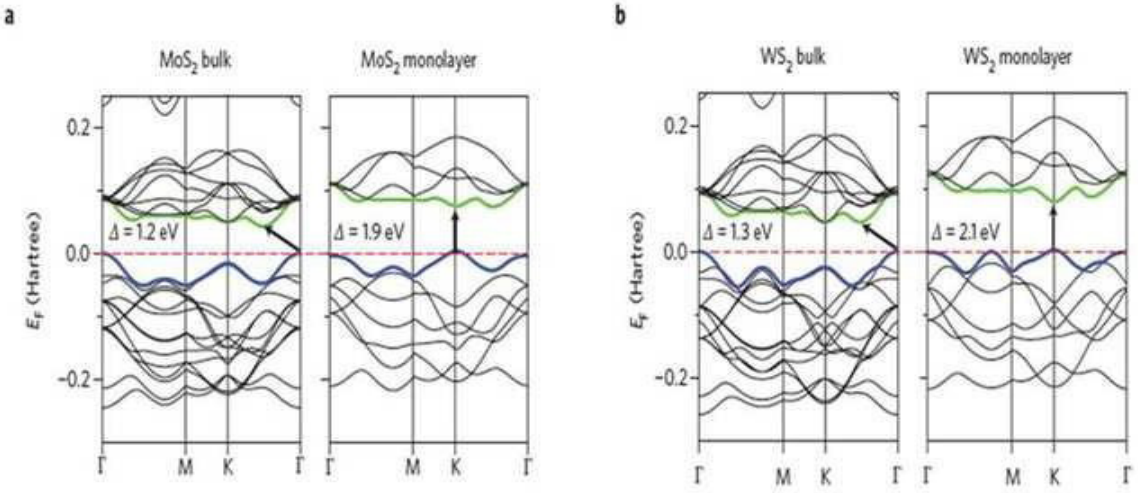

Figure 3-8: The band structure of TMDCs. Band structures are calculated by DFT (density functional theory) for multilayer and monolayer MoS_2 (a) and WS2 (b) [42-43].

Table 3.2 Prohibited indirect (Egind) and direct (Egdir) bands for the four lamellar compounds studied in our work at room temperature. [44]

Material	***Forbidden band indirect (ev)***	***Forbidden band direct (ev)***
WS_2	1.3	2.04
MoS_2	1.25	1.90

5.2. Absorption spectrum, refractive index and transmittance

Like graphene, the physical properties of transition metal dichalcogenides (TMDCs) change dramatically as the thickness of the material is reduced to a monolayer (ML). Thus the two-dimensional semiconductors of the MoS_2 family, MoSe2, WS2 and WSe2 have a direct gap in the visible spectrum and exhibit a high optical absorption (> 10% / ML) [45]. They have a high potential for electronic devices (transistors) and optoelectronics (photodetectors, LEDs or solar cells).

These materials are characterized by an indirect energy band of 1.1-1.3 eV and direct transitions from 1.6-2.0 eV.

Direct transitions are associated with Wannier excitons (delocalised) with binding energies of the order of 50 to 100 meV [11]. These high exciton binding energies imply that, even at room temperature, the eccitonic structures are visible in the spectra of optical constants. Figure (3.9) shows the refractive index n and the absorption coefficient α of a monocrystal of WS_2 determined by ellipsometry. Peaks A and B are associated with excitonic absorption. Above 1.92 eV, the value of α is greater than 10^7 m^{-1}, which means that at least 90% of the light intensity is absorbed over 0.23 μm. Between 1.5 and 3 eV, the refractive index n varies between 3.5 and 5.

The crystalline anisotropy of the lamellar compounds leads to anisotropy of the optical properties.

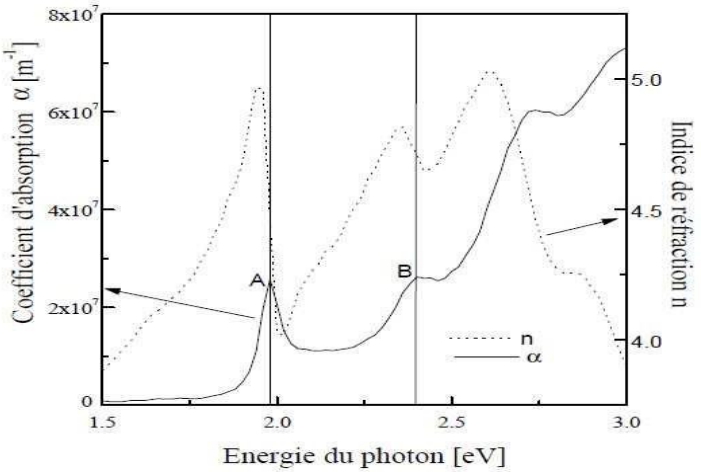

Figure 3-9. Optical absorption coefficient α and refractive index *n* of WS_2 at room temperature. *n* and α were determined by ellipsometry on a monocrystal of WS_2 [33]

For semiconductors with a direct forbidden band of photons with energy greater than band gap energy can be easily absorbed or emitted. On the other hand, for those with an indirect gap band, an extra phonon must be absorbed or emitted for the sake of crystal conservation, the absorption of photons or an emission process is much less efficient.

6. ELECTRICAL PROPERTIES OF TMDCs

Unlike semiconductors commonly used in microelectronics such as Si, GaAs or Ge, it is difficult to obtain precise data on the key parameters of the lamellar semiconductors, for example on the intrinsic mobility, the doping possibilities, the effective masses, ...This is partly related to the difficulty of preparing single crystals.

Even using base materials of the same nominal purity (99.9999% purity) but from different sources, the type of doping, mobility and conductivity of the single crystals obtained may be completely different [40], it is for this reason that the mastery of the techniques of elaboration of these materials is necessary.

a. Conductivity and mobility

The anisotropic crystalline structure of the lamellar compounds leads to anisotropy of conductivity and mobility.

The doping of TMDCs

The doping in transition metal dichalcogenides is generally a redox reaction consisting of introducing, by electrochemical or chemical means, accepting species (p-type doping carried out by oxidants) or electron donors (doping type n made by reducers) between the layers of MX_2 [46] of semiconducting nature.

In the particular case of MoS_2 and WS_2, it seems that an excess of sulfur anions induces a p-type conductivity whereas a lack of sulfur results in a conductivity of the type.

However, there is no model that reliably predicts the type of doping and carrier concentrations obtained by adding elements given during growth. Even without intentional doping, the single crystals are generally doped (n or p), with carrier concentrations [33] of the order of 10^{21} to 10^{24} m^{-3}.

Table 3.3: the electrical transport properties of a hexagonal structure of MoS_2 and WS2 of type n and p. [36]

Material	o_T (S cm^{-1})	$n_{e,p}$ (cm^{-3})	$\mu_{e,p}$ (cm^2/Vs)	E_a(eV)	S (µV K^{-1})
n-WS_2	25	1,2-2,4.10^{15}	103-150	0,25	
p-WS_2	0,03-6,67	0,2-5,9.10^{15}	70-290	0,10	
n-MoS_2	0,6-7,9	≈2.10^{17}	2-200	0,07-	
p-MoS_2	0,01-4,2	1,8-3,0.10^{17}	86	0,16 0,015	360-580

To know o_T is the electrical conductivity perpendicular to the axis c, $n_{e,p}$ is the electron density of electrons and holes, $\mu_{e,p}$ is the mobility of electrons and holes, E_a is the activation energy and S is the coefficient of seebek.

The effect of doping on the charge carriers

The friable structure of these materials due to the nature of the chemical bonds between the sheets [X-M-X] induces a strong electron-phonon coupling. A charge introduced during the doping causes a local deformation of the chain and creates a state located in the forbidden band; we then speak of localized defects.

Indeed, these quasis particles (defects + charge) cause a disorder in the crystal. This disorder has the effect of the location of electronic states particularly drastic low dimension. The causes of disorder are manifold and manifest at different scales. We will speak of homogeneous defects at the molecular level and of heterogeneous disorder for microscopic and macroscopic scales [46]. The organization of the material, therefore the quantity and type of defects encountered, is decisive as regards the properties of the conduction. The chemical synthesis mode and the formatting intervene critically in the existence of the order within MX2.

The anisotropic crystalline structure of the lamellar compounds leads to anisotropy of conductivity and mobility. The measured ratios of anisotropy sometimes very high are to be put on the account of stacking defects and their power of diffusion carriers. The high anisotropies measured on certain single crystals are therefore extrinsic in nature. For example, creating defects when handling samples.

The effects of defects on physical properties

In the materials we study in our work inevitably there exist defects whose origin is quite varied. Irradiations cause many displacements of atoms in the crystal. At each vacant site corresponds an interstitial atom located in a Van der Waals gap: these are Frenkel defects. The disorder thus introduced, causes a significant modification of the physical properties of these materials. The local conditions of screening around a fault modify the electronic distribution and affect the charge density wave. Beyond a critical density of defects, the phase transitions disappear and there remains only an incommensurable phase, corresponding to a disordered structure.

Another type of defects is obtained by doping or substitution. We recall the main results:

- Creation of defects in the sub-networks of anions, for example by replacing a portion of the atoms of selenium by sulfur atoms. This does not remove these phase transitions.
- Except for the defects obtained by substitution, the techniques used for the creation of defects such as neutron irradiation and irradiation with very high energy electrons. These irradiations have interesting advantages: homogeneity of the defects created, and concentrations of defects controlled, but when they are very low.

By irradiation with high energy particles, gaps are created in the atomic planes of the transition metal and lodge in Van der Waals gaps between the layers. In this case 1% [46] of displaced atoms are enough to destroy the phase transitions.

This shows the importance of the nature of the defects created. The charge density wave is much more affected, due to the great influence of the fault on the electronic system.

b. The diffusion length and the life expectancy

There is little data on LD diffusion lengths and temps life times in MX2 semiconductors (M = Mo, W, X = S). Typical diffusion lengths have as order of magnitude *LD*c = 10-200 µm in the WS_2 along the sheets and a few micrometers perpendicular to the sheets.

7. THE MECHANICAL AND CHEMICAL PROPERTIES

MX2 lamellar materials (M = Mo, W, X = S) have long been used as solid lubricants, they have good properties to reduce friction through easy cleavage between sheets. Nevertheless, the environment in which the layers of these latter materials are used influences their performance. Thus, in the case of a contact between two metal surfaces lubricated by a MoS_2 coating, the coefficient of friction increases with humidity up to 65% RH, and then decreases [47]. An increase in contact pressure or speed results in a decrease in the

coefficient of friction. Indeed, at high pressure or speed, there would be heating up in the contact

Causing evaporation of water present between MoS_2 films. The durability of the film is largely controlled by the moisture content.

The increase of the coefficient of friction with moisture is generally attributed to the formation of hydroxides or oxides of molybdenum (MoO_3) or tungsten (WO_3).

It is also conceivable that the water molecules react with the pendant bonds of the crystallite edges, thus hindering the relative movement between the sheets or their rotation in the contact.

With regard to the chemical properties these materials are chemically stable and have an active resistance to photocorrosion [49].

Other properties are shown in the following table

Table 3. 4: Direct gap band, the effective mass of electrons, dielectric constant for a monolayer of MX2 [48]

MX2	**Gap band (ev)**	**m_e^*/m_e**	**constant dielectric**
MoS_2	1.8	0.56	4.8
WS_2	1.93	0.33	4.4

III.II INTRODUCTION TO THE PROPERTIES OF GRAPHENE

1. INTRODUCTION

Graphene is the name given to the single layer carbon sheet (Fig. 3.10) which was isolated experimentally for the first time in 2004 [50]. Before that, graphene had been investigated theoretically for over sixty years, although its existence as a 2D crystals in free space was thought impossible [51]. In the last eight years graphene has been the most studied material in the world, attracting the attention of the entire scientific community for its fascinating physical and chemical properties.

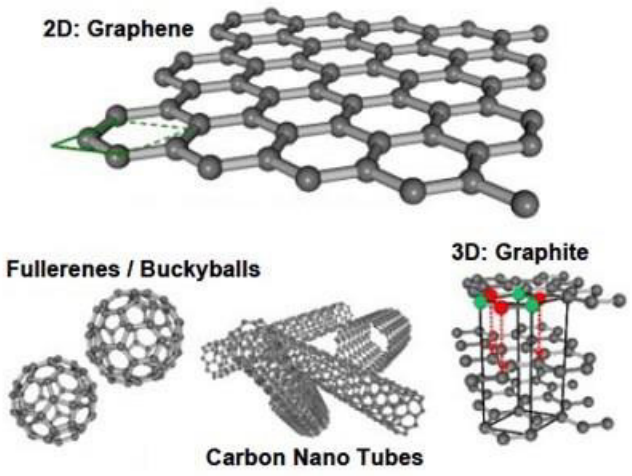

Figure 3-10: Graphene structure compared with other carbon materials: fullerenes, carbon nanotubes and graphite. Image taken from [52].

Graphene shows such a different behaviour to be considered as a new material. The electronic properties of graphene are probably one of its most interesting and studied aspects. First of all, graphene has been the first material showing electronic linear dispersion (see next section). The charge carriers show remarkably high mobility, this ensures that they can travel for sub-micrometer lengths undergoing few scattering events. Graphene can also be considered as a giant molecule and thus, it can be used for chemical functionalization as a basis for building new materials. Today graphene is considered to have big potential in the world of applications: as

a transparent, flexible and conductive material it is very promising for microelectronic and optoelectronic devices [53].

In this chapter some of the properties that make graphene a unique material are discussed, followed by an overview of the aims and structure of this thesis.

2. GRAPHENE BAND STRUCTURE

In carbon materials, excluding the diamond where electrons are hybridized in a sp^3 configuration, the π valence electrons are responsible for transport, magnetism and other physical properties. What makes graphene really special is first of all the uniqueness of its band structure.

Fig. 3.11 (a) and (b) show the unit cell in the real lattice and the Brillouin zone in the ciprocal lattice of the 2-D system, respectively.

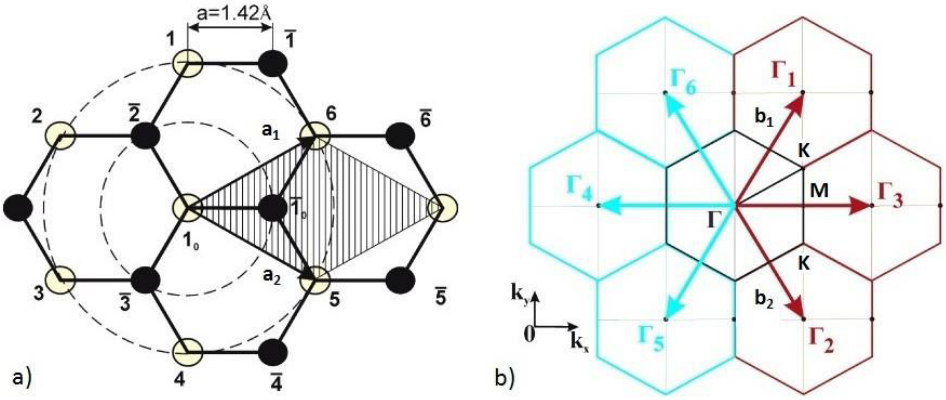

Figure 3-11: Real (a) and reciprocal (b) lattice of graphene.
Image adapted from [54].

The unit vectors in the real space are given by:

$$\mathrm{a}_1 = \left(\frac{3a}{2}, \frac{\sqrt{3a}}{2}\right) \qquad \mathrm{a}_2 = \left(\frac{3a}{2}, \frac{\sqrt{3a}}{2}\right) \tag{3.2}$$

where the graphene lattice constant is $|\,\mathbf{a_1}\,| = |\,\mathbf{a_2}\,| = 2.46\,\mathring{\mathrm{A}}$. In the reciprocal lattice the unit vectors are:

$$\mathrm{b}_1 = \left(\frac{2\pi}{3a}, \frac{2\pi}{\sqrt{3a}}\right) \qquad \mathrm{b}_2 = \left(\frac{2\pi}{3a}, -\frac{2\pi}{\sqrt{3a}}\right) \tag{3.3}$$

The high symmetry points Γ, *M* , *K*, indicated in Fig. 3.11 (b),

correspond to the center, corner and center of the edge of the first Brillouin zone.

The theory which is adopted to calculate the electronic band dispersion is the tight binding method (see reference [55]). The Hamiltonian equation problem can be solved by considering the nearest neighbour atom.

In particular, the simplified energy dispersion relation, which is plotted in Fig. 3.12, is the following:

$$E_{g2D}(k_x, k_y) = \pm t\{1 + 4\cos\left(\frac{3k_x a}{2}\right)\cos\left(\frac{k_y a}{2}\right) + 4\cos^2\left(\frac{k_y a}{2}\right)\}^{1/2} \quad \text{..... (3.4)}$$

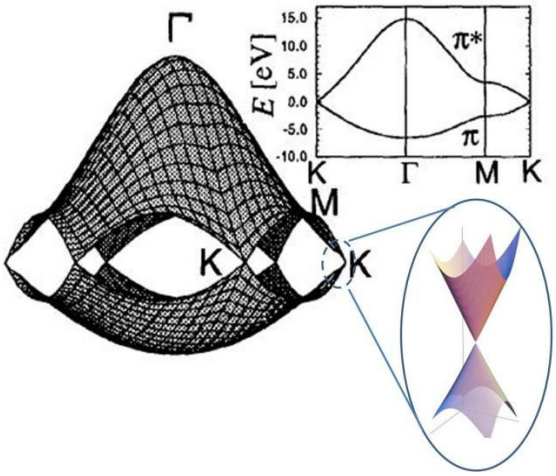

Figure 3-12: Graphene energy dispersion bands plotted for the whole region of the Brillouin zone. The top-right inset shows the dispersion along the high symmetry directions Γ, *M, K*. In the bottom-right inset, the linear dispersion occurring at the *K* points is magnified. Image adapted from [55-56].

The term *t* is called the *nearest neighbour hopping energy*, with a value of about 2.8 *eV*. The signs ± are related to bonding and anti-bonding *π* energy bands. The most interesting transport properties of graphene are due to the dispersion around the *K* points (bottom-right inset of Fig. 3.13). By expanding equation 3.3 around these regions it becomes:

$$E^{+}_{linear} = \pm \hbar v_F |k| \quad (3.5)$$

where v_F is the Fermi electron velocity, equal to ~ $10^6 m/s$ in graphene. For the electron bands behaviour around the *K* points, graphene is

considered a gap-less semiconductor. It is possible to make a parallel connection between graphene elec- trons and relativistic particles: the linear dispersion relation 3.4 reduces to the Dirac equation if the electron mass is set to zero and if v_F substitutes of the speed of light c.

This is the reason why the charge carriers in graphene can be treated as massless Dirac particles [56].

3. DENSITY OF STATES

From the E(k) linear dispersion relation it is possible to derive the *density of states* (DOS) which can be defined as the number of energy eigenstates in a unit energy interval [30]. Mathematically, this is equivalent to:

$$\mathrm{g(E)}dE = 2gz\left(\frac{dA}{(2\pi)^2/\Omega}\right) \ldots\ldots\ldots\ldots\ldots\ldots\ldots\ldots\ldots\ldots\ldots\ldots (3.6)$$

where g_z relates to the zone degeneracy. As there are six K points, each one shared by three atoms, g_z = 2 and Ω is the area of the reciprocal lattice. dA is an infinitesimal area in the k-space and as the perimeter can be written as $2\pi k$ it follows that $dA = 2\pi k dk$. Finally, the expression for $g(E)$ normalised by the total area Ω is:

$$\mathrm{g(E)} = \frac{2}{\pi}\left|\frac{kdk}{\mathrm{dE}}\right| = \frac{2}{\pi}\left|\mathrm{k}\left(\frac{dE}{\mathrm{dk}}\right)^{-1}\right| \ldots\ldots\ldots\ldots\ldots\ldots\ldots\ldots\ldots\ldots\ldots\ldots (3.7)$$

Using the 3.4 the previous expression becomes:

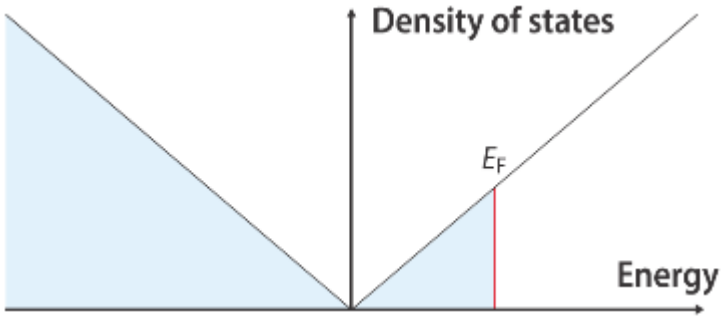

Figure 3-13: Density of states near the Fermi level with Fermi energy E_F. Image taken from [58].

$$g(E) = \left(\frac{2}{\pi(\hbar v_F)^2}|E|\right) = \beta_g|E| \quad \ldots\ldots\ldots\ldots\ldots\ldots\ldots\ldots\ldots\ldots\ldots\ldots\ldots\ldots (3.8)$$

The linear energy dependence of the density of states is shown in Fig.3.14 and the value of β_g is $\approx 1.5 \cdot 10^{14} eV^{-2} cm^{-2}$. At the Fermi energy $E_F = 0$ the density of states is zero; therefore graphene can be considered a gap-less semiconductor.

4. GRAPHENE MECHANICAL PROPERTIES

The melting temperature of thin films decreases with the layer thickness and for significantly reduced thicknesses (≈ tens of atomic layers) the films tend to become unstable. This is the main reason why 2D materials such as graphene were thought impossible to exist. Graphene was found to be not just thermodynamically stable up to high temperatures, but also the strongest material ever existing. The origin of graphene's robustness lies on the *σ bonds* which connect the carbon atoms in a solid honeycomb packed structure. Importantly, graphene flakes obtained by mechanical exfoliation of graphite have a very good crystalline quality [58]. The strength of the atomic bonds ensures the absence of dislocation or other crystal defects. This is also confirmed by the high performances shown by the charge carriers which can travel thousands of interatomic distances without scattering.

AFM nanoindentation measurements have been performed to probe the elastic stress-strain response [59]. In defect-free graphene sheets, a stiffness of the order of 300 − 400 *N/m*, with a breaking strength of ca. 42 *N/m*, have been reported.

The latter value is about 200 times greater than the one measured in steel. The estimates of the Young's modulus yielded approximately 0.5 − 1.0 *T P a*. These values, combined with the relative low cost of thin graphite, make this material an ideal candidate for mechanical reinforcement as suggested in [61]. In addition, due to its exceptional elastic properties, graphene will be implemented soon in bendable electronic devices such as transparent and stretchable screens, displays, sensors and antenna [62,63].

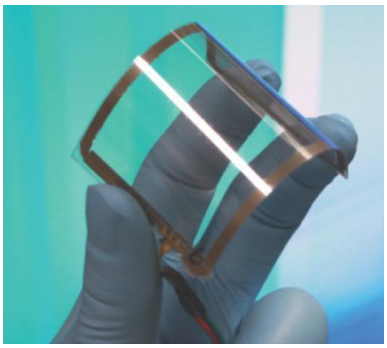

Figure 3-14: Graphene on polyethylene terephthalate (PET), assembled in a touch panel which shows outstanding flexibility. Image taken from [62].

5. GRAPHENE FUNCTIONALIZATION

Graphene is a chemically inert material. Nevertheless, the existence of an atom- ically thin material has introduced the possibility of performing chemical modifi- cation with the aim of achieving new 2D graphene-based derivatives. Despite the close relationship with graphene, these materials show very different properties due to the change of their electronic structure.

Fluorographene [64], for instance, is a new material where *F* atoms saturate the *C atoms* in a sp^3 hybridization configuration (see Fig. 3.15(a)). It inherits high mechanical strength from graphene but, differently unlike the pristine carbon sheet, it is a high quality insulator. Resembling Teflon properties, fluorographene is very inert below 400°C. From an applications point of view, fluorographene seems a promising insulator material to be implemented in graphene heterostructures.

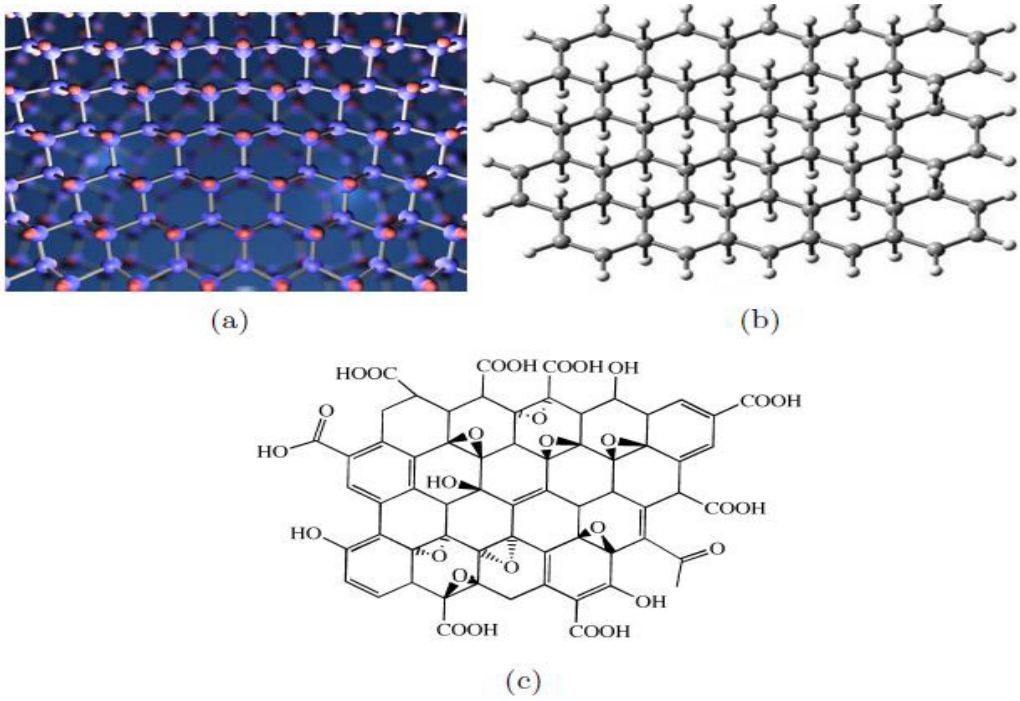

Figure 3-15: (a) Fluorographene atomic structure: every *C* atom of thegrapheme lattice (blue spheres) is bonded with a *F* atom (red spheres), in a sp^3 hybridization configuration. (b) Molec- ular representation of fully hydrogenated graphene. (c) Idealized graphene oxide structure where the oxygen functional groups are oriented out of the graphene plane.
Images taken respectively from [65-66 and 67].

The exposition of graphene to hydrogen plasma leads to a new material called graphane, where each carbon atom is bonded to a hydrogen atom [68]. However, differently from fluorographene, graphene hydrogenated either in one or both sides looses hydrogen atoms at moderate temperatures. This lack of stability causes doubts about possible applications of this material.

Graphene Oxide [69] is another insulating graphene derivative obtained by oxidation of the graphene lattice. In this case the structure is not stoichiometric and, as shown in Fig. A.4 (b), the oxygen functional groups (epoxide, carbonyl, hydroxyle, phenol) are randomly attached outside the graphene plane at both sides. Graphene oxide is less stable than fluorographene, showing reversibility to the unoxidized state by thermal or chemical reduction [70, 71]. A recent finding, which may lead to important applications, is the use of graphene-oxide as a selective membrane through wich only water molecules can pass through [72].

Chapter IV

SILVACO ATLAS (TCAD) Simulation and Results

IV. SILVACO (TCAD) SIMULATION AND RESULTS

IV.I SILVACO ATLAS (TCAD) SIMULATION TOOL

1. INTRODUCTION

In our work, we used technological simulation software **SILVACO (TCAD)**, to simulate the electrical and optical characteristics of 2D Materials III-V materials junction solar cell. A detailed structure is made of Schootcky diode graphene/semiconductor, MoS_2/semiconductor. First, we should learn some basic notions and how it works this software and then we would proceed to our simulation and discuss the results that we obtained from our work.

2. THE ROLE OF SIMULATION

Device simulation helps users understand and depict the physical processes in a device and to make reliable predictions of the behavior of the next device generation. Two-dimensional device simulations with properly selected calibrated models and a very well-defined appropriate mesh structure are very useful for predictive parametric analysis of novel device structures. Two- and three-dimensional modeling and simulation processes help users obtain a better understanding of the properties and behavior of new and current devices. This helps provide improved reliability and scalability, while also helping to increase development speed and reduce risks and uncertainties.

The simulation gives us the opportunity to link the theoretical and experimental wolds with impossible mathematical analyzes, and giving us space to build a physical world with certain conditions.

3. A BRIEF HISTORY ABOUT SILVACO

Silvaco, (Silicon Valley Corporation). Develops and markets electronic design automation (EDA) and technology CAD (TCAD) software and semiconductor design IP (SIP).

It is a leading provider of professional chains of finite element simulation and computer-aided design software for the Technology Computer Aided Design (TCAD)

The company is headquartered in Santa Clara, California, and has a global presence with offices located in North America, Europe, and throughout Asia. Since its founding in 1984 by Dr.Ivan Ppesic, Silvaco has grown to become a large privately held EDA company. The company has been known by at least two other names: Silvaco International,[73] and Silvaco Data Systems.[74]

In 2003 Silvaco acquired Simucad Inc., a privately held company providing logic simulation EDA software. Silvaco re-launched the brand by spinning out its EDA product line in 2006 under the Simucad name.[75] As of February 17, 2010, Simucad Design Automation and Silvaco Data Systems were merged back together forming Silvaco, Inc.[76]

In 2016, Silvaco added semiconductor design IP (SIP) to its portfolio with the acquisition of the privately held company IPextreme, Inc.[77] Silvaco also entered into another new market segment with the acquisition of the privately held company edXact in France.[78] The tools from edXact are used for analysis, reduction, and comparison of extracted parasitic netlists.

In 2017, Silvaco acquired SoC Solutions, a privately held company providing semiconductor IP.[79]

4. SILVACO (TCAD) SOFTWARE:

- **The VWF: (virtual wafer Fab)**

VWF enables users to perform advanced analysis tasks like Design of Experiments (DOE) or optimization, using any of the Silvaco simulators.

There are a lot of software that form VWF but the famous is Atlas and Athena, these tools are divided into two main categories

- **Main Tools** and **Auxiliary tools**

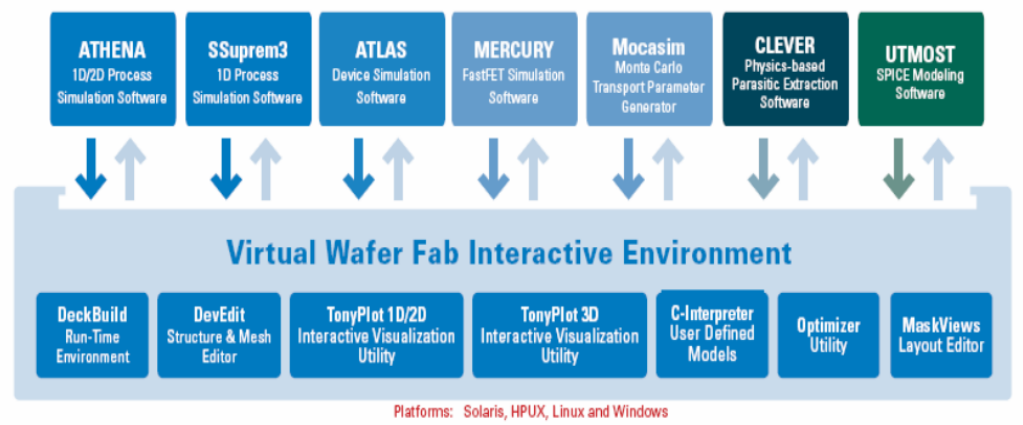

Figure 4-1: The Virtual Wafer Fabrication [80].

Atlas:

Atlas is a 2D and 3D simulator that performs AC and AC analysis and transient analysis of most semiconductor-based devices. Atlas allows identifying and optimizing the characteristics of semiconductor devices for a wide range of technologies. In addition to the "external" electrical behavior, it provides information on the internal distribution of variables such as carrier concentrations, electric field or potential, etc., all important data for the design and optimization of technological processes.

ATLAS has been designed so that it can be used with other tools that facilitate or supplement its use.

This simulator consists of two parts:

- A Digital Processing Part (method of integration, discretization ...).
- A part formed of the physical models of the most recent semiconductor components: models of recombination, impact ionization, mobilities, temperature and statistics of Fermi-Dirac and Boltzmann in particular.

The diagram in Figure 4.2 shows the different types of information that circulate at "Atlas" inputs and outputs. Most simulations carried out under "Atlas" use two input files [80]

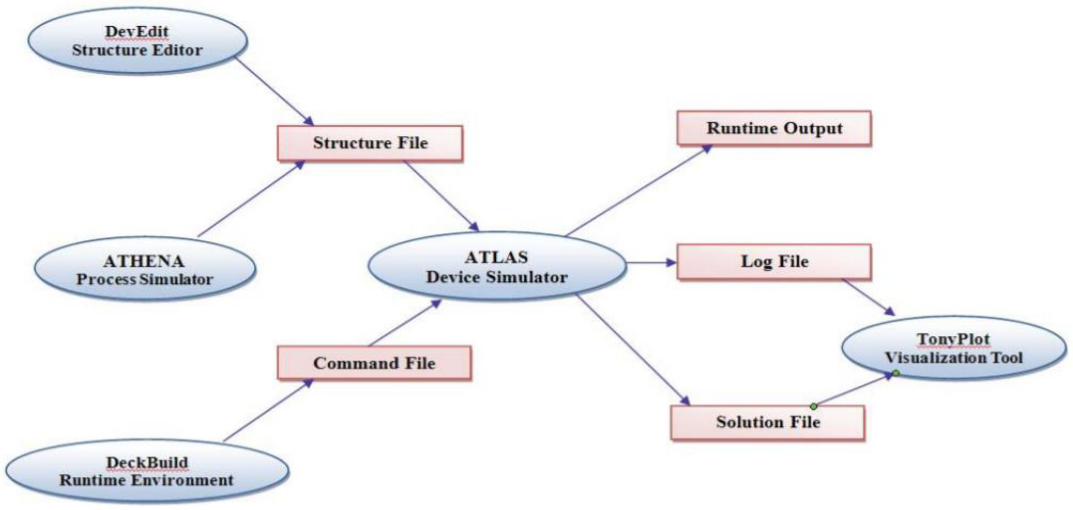

Figure 4-2: shows the flows of information to and from the Atlas simulator [80].

The first file is a text file containing commands for "**Atlas"** to run (represented by "Command File"). The second file is a "structure file" containing the structure of the device to be simulated defined in "**Athena**" or "**DevEdit**".

At the "Atlas" output, we have three types of files. First one is is the "**Runtime**" output, which gives progress, errors and warning messages during the simulation. Secondly is the "**log**" file, which stores all voltage values and currents from the analysis of the simulated device. Third is the "**Solution File**", this file stores the 2D or 3D data concerning the values of the solutions variables at a given point of the device.

ATHENA is simulation software including in SILVACO and is used for simulating the manufacturing process of the different constituents of an electronic device, and also treats ion implantation and diffusion of impurities and oxidation and other technological processes of manufacturing. It is generally used to simulate simultaneously With Atlas.

DEVEDIT is an environment where the structure (dimension, doping,) and its mesh are drawn.

DECKBUILD is an environment where the simulation program is defined as shown in Figure 4-3.

TONYPLOT is an environment where the simulation results are displayed (structure of the component, distributions of various quantities in it, electrical characteristics ...).

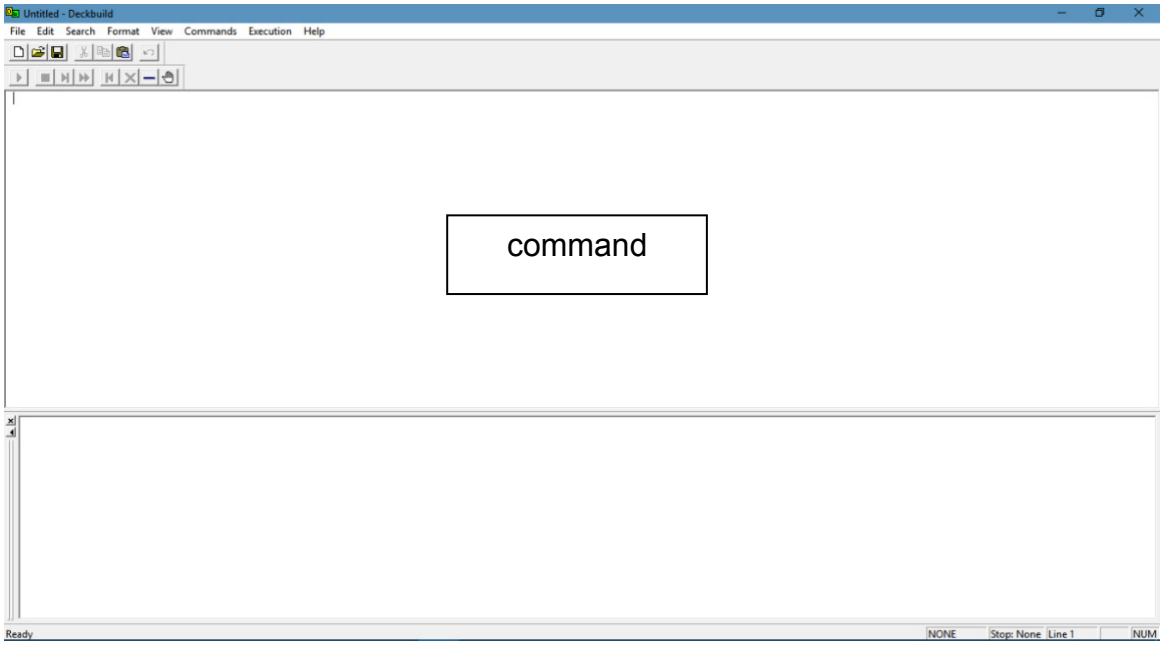

Figure 4-3: duck build window

4.1 Atlas Operating Mode:

The command is entered in DECKBUILD by go atlas lik the picture shown above.

The Order of Atlas Commands

The order in which statements occur in an Atlas input file is important. There are five groups of statements that must occur in the correct order Otherwise, an error message will appear, which may cause incorrect operation or termination

of the program. For example, if the material parameters or models are set in the wrong order, then they may not be used in the calculations.

The order of statements within the mesh definition, structural definition, and solution groups is also important. Otherwise, it may also cause incorrect operation or termination of the program.

4.1.1 Syntax of an instruction:

An instruction takes the following general form:

```
<Instruction><parameter> = <value>
```

There are 04 types for values (real, integer, logic, character)

The order of parameters is not mandatory; abbreviation is possible but requires no overlap with other instructions.

To write a comment that is not executed by the compiler, we use the symbol **#**.

ATLAS can read **256** characters in a line, but it is better to separate the lines with a backslash at the end of the line in a long statement so that the instructions can be read in a clear way.

It does not differentiate between a capital letter and a lowercase letter.

4.1.2 Instructions' order:

After the presentation of the **"Atlas"** simulation tool of **SILVACO TCAD**, its internal composition and its functioning we will now present the order of Commands specific to Atlas programming logic. Thus, there are five groups of commands, these groups must be organized correctly (Figure 4.2). If the order is not respected, an error message appears and the program does not execute correctly. For example, if the parameters or material models are not placed in the proper order, the simulator does not consider them.

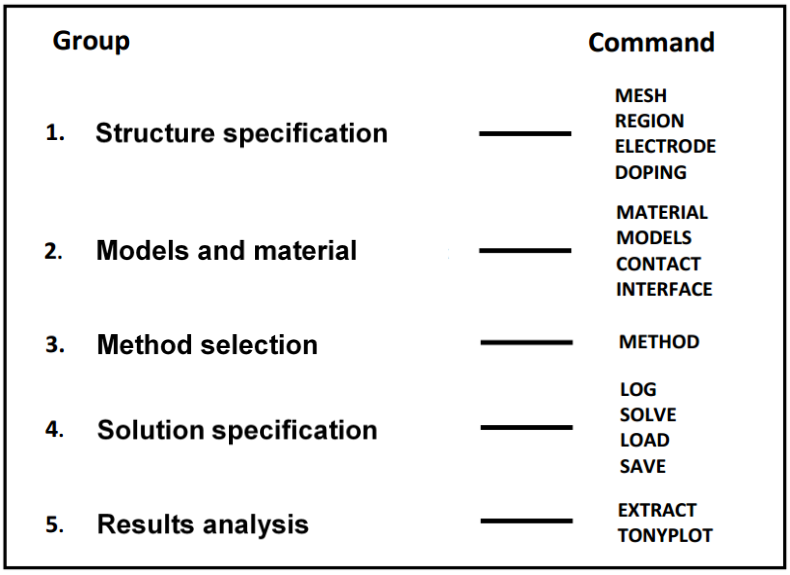

Figure 4-4: Order of groups of Atlas commands (The associated basic commands) [80].

ATLAS is a powerful tool, its instructions are very numerous and its documentation is voluminous that it is difficult to explain everything about it in this thesis.

In order to explain the ATLAS tool, we found that it is useful, in our framework, to illustrate the operation of this tool with the help of concrete examples. We will therefore give an example of simulation of **a solar cell graphene / MoS_2 / n-Si at Schottky junction**, by explaining the construction process of its structure in **DECKBUILD** and putting it under solar lighting with **AM1.5**, and by studying its characteristics.

The instructions will be illustrated in the rest of this chapter, as well as the results of our simulation.

The following figure represents the structure of the Graphene/MoS_2 solar cell that we want to simulate in ATLAS.

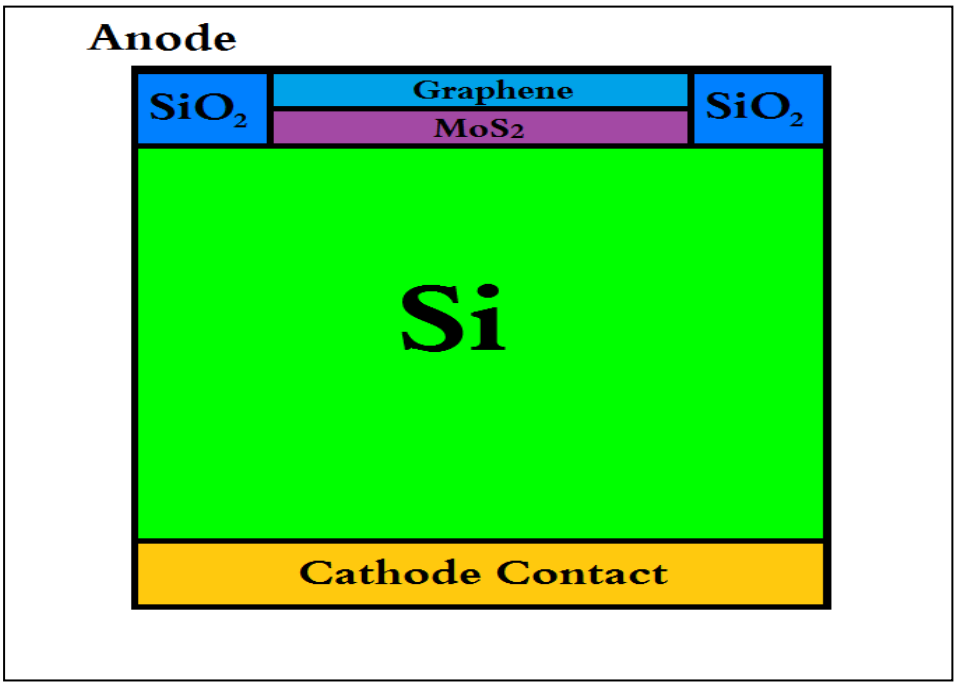

Figure 4-5: The structure of our graphene / MoS_2 / n-Si solar cell that we want to simulate in SILVACO TCAD.

4.2 Structure Specification:

The specification of the structure is obtained by identification of **mesh, regions, electrodes and the doping.**

4.2.1 MESHING

The first section of structure defining statements in the Deckbuild program is themeshing section. This section specifies the two-dimensional grid that is applied tothedevice with mesh statements.

The following instruction is used to define the meshing:

```
x.mesh location=<value> spacing=<value>
```

The ATLAS device simulator can more easily solve the differential equations at each grid point if there are no abrupt changes between adjacent points. Mesh statements have two parts called location statements and spacingstatements.

The location statement, "`loc`", specifies the x or y value in the structure to whichthe following "spacing" statement is applied.

The spacing statement, “spac”, specifies thespacing between grid lines at that specific location.

The Figure 4-6 represents the meshing that we have created for our structure and its respective instructions entered in DECKBUILD.

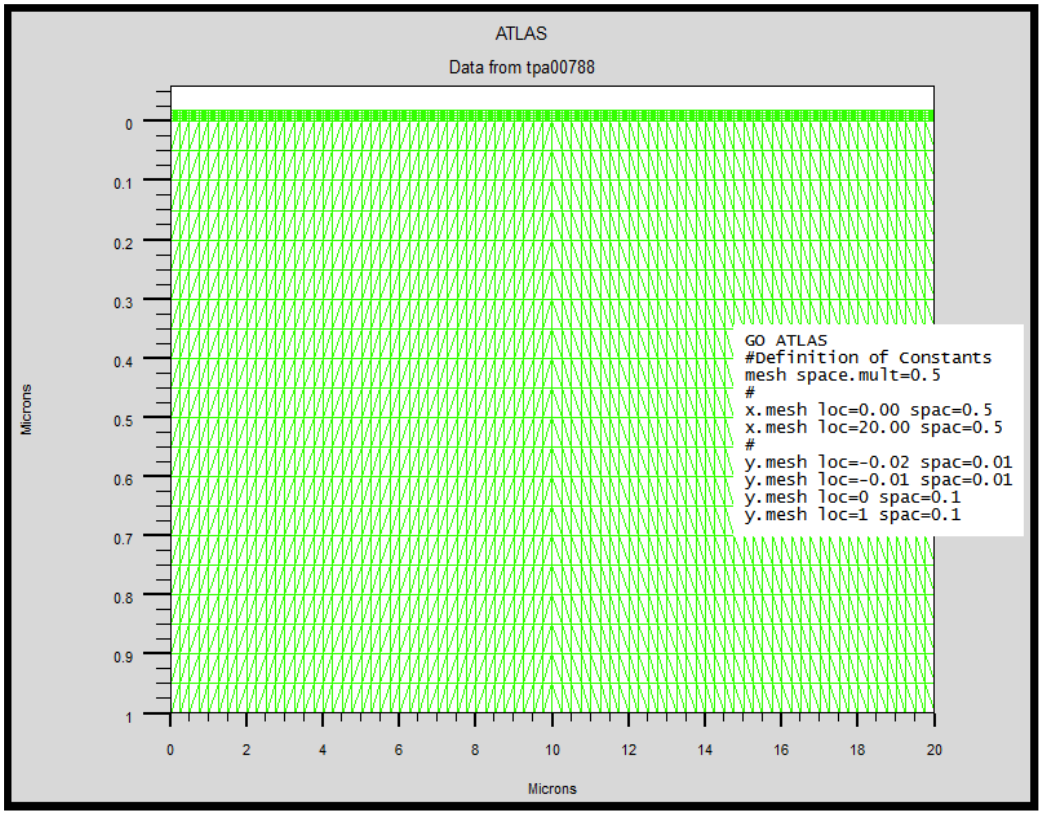

Figure 4-6: The mesh statements creating the mesh for the graphene solar cell / MoS_2 / n-Si are displayed along with a picture of the created mesh

4.2.2 REGION

The region statements include a region number, a material specification, and the region boundaries. The region number is arbitrary but is used in later structure specification sections to apply characteristics to certain regions.

The instruction for defining regions is as follows:

```
REGION number=<integer> material=<material_type> / <position_parameters>
```

Every region must have a different number as the program produces an error if a statement applies to two different regions.

The material specification statement specifies that the whole region consist of the stated material. This statement gives that whole region default parameters and characteristics of that specified material, which are stored in the **ATLAS material library**. These values include parameters such as the bandgap, electron and hole mobility, and optical properties such as the index of refraction.

P.S: These parameters can be used or changed in another section of the structure defining code if the user wishes to modify a material's original properties**.**

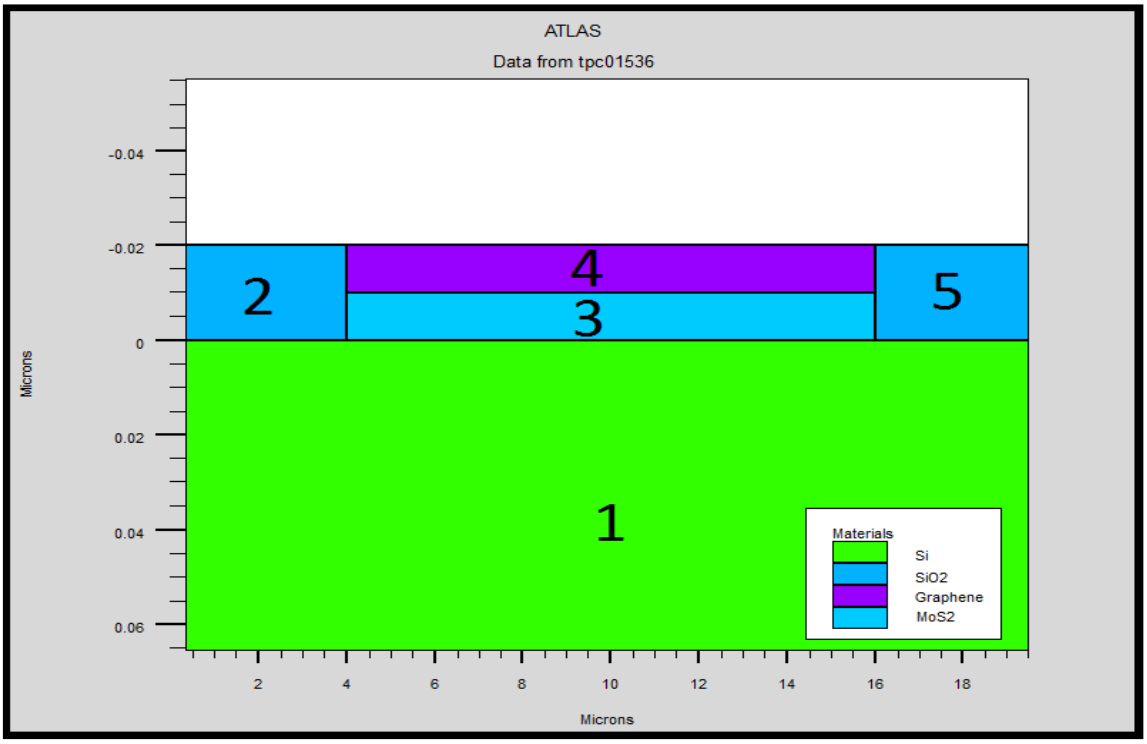

Figure 4-7: The region statements creating the regions of the solar cel graphene / MoS_2 / Si are displayed along with a picture of the created regions.

Graphene, as a material, is not included in ATLAS material library, so to define it, we used the statement “user.material”, which is used to define materials unknown to ATLAS, and we allocated it to its respective region with the position parameters.

The color code is used to identify the materials (each material corresponds to a color), while vertical and horizontal lines mark the boundaries of each region.

There are four specific areas. Each area is defined by a color, and its

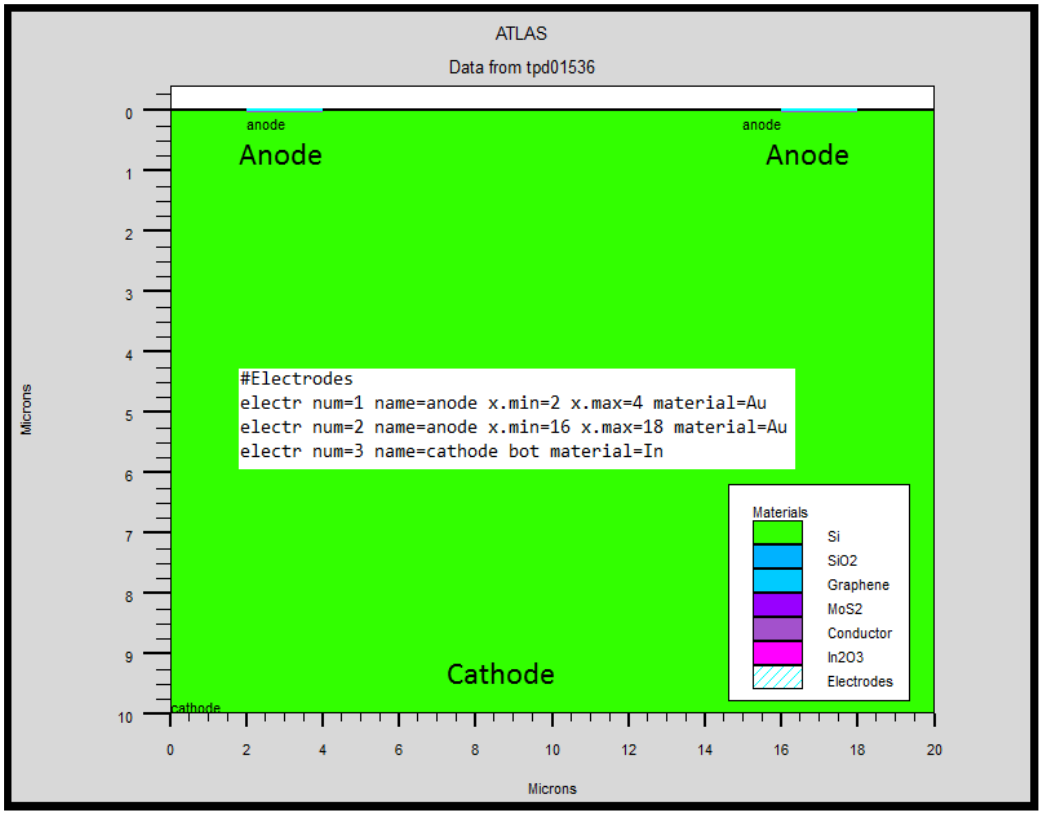

Figure 4-8: A magnified section for areas with specific materials

4.2.3 ELECTRODES

The definition of electrodes is as follows:

```
Electrode Name=<Electrode Name><position_parameters>
```

The user has the ability to determine any number of electrodes with different metal properties. Each electrode definition statement usually has three parts. The user must first name each pole. The name can be followed by the “material” statement, which is used to determine the type of contact metal that is used as electrode, which can be one of the materials registered in ATLAS

Material Library, or a user-defined material, like in our case where we used Graphene as Anode.

The statement for the definition of an electrode uses maximum and minimum limits of x and y values to set the limits of each electrode. The positions of the electrodes are located by the following instructions:

`X.MIN`: Specifies the starting point of the electrode.

`RIGHT`: the position of the electrode is located to the right of the structure (inverse: LEFT).

`TOP`: the position of the electrode is at the top of the structure (inverse: BOTTOM).

It is also possible to name the electrode only and identify it as covering the top or the bottom of solar cells.

In our example two anodes at the top of the structure with a length of 2 μm each, and a cathode at the bottom of the structure translated by the following instructions in Figure 4-8

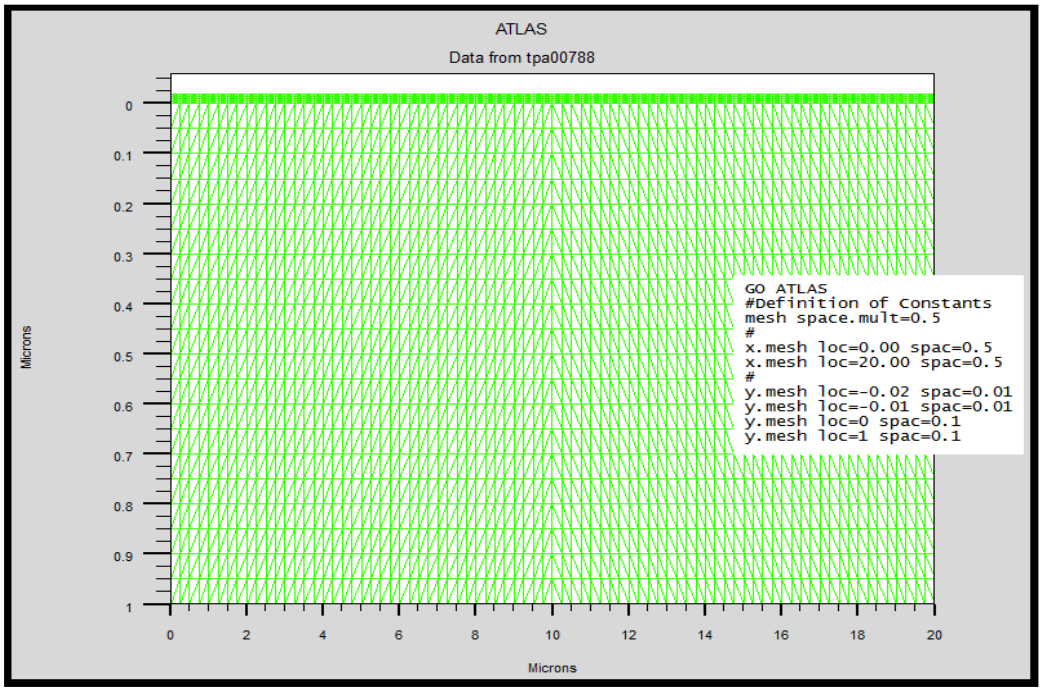

Figure 4-9: The cathode and the anode are made together with the electrode identification code in the graphene / MoS_2 / Si solar cell.

4.2.4 DOPING

The last aspect of structure specification that needs to be defined is doping. The format of theAtlas statement is as follows:

```
DOPING <distribution type><dopant_type><position parameters>
```

In our work, we used a doping with a uniform n-type distribution and different donor concentrations.For example, the instructions of a donor concentration of 1.e16 cm^{-3} with a uniform distribution for the Si substrate is given by:

```
Doping n.type conc=1.e16 uniform region=1
```

Once the structure defined, it can be saved in a **.str** file. This can be accomplished by the following statement:

```
save outf= Graphene_MoS2_n-Si.str
```

On the other hand, we can view the design of the structure using the **Tonyplot** tool using the following statement:

```
Tonyplot Graphene_MoS2_n-Si.str
```

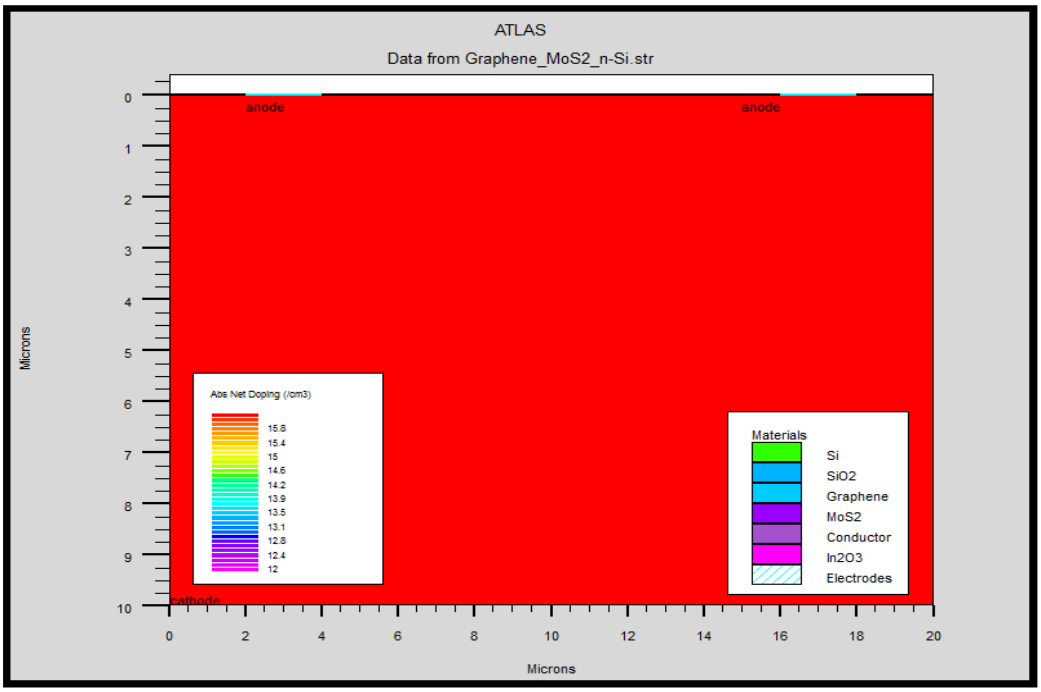

Figure 4-10: graphene / MoS_2 / Si solar cell dope n type.

4.3 Materials and Model Specification:

After specifying the mesh and doping, we can easily modify the characteristics of the materials used (electrodes, substrate) and change their parameters that ATLAS takes them by default and define our choice of the physical model that will be used during the simulation. These actions are accomplished by the following instructions: MATERIAL, CONTACT, and MODELS.

4.3.1 MATERIAL

The material defining statements that follow the definition of the device structureallow the user to alter the properties of given materials or to input newmaterials into the device. The statements alter the material properties of a specifiedmetal, semiconductor, or insulator, to simulate more accurately a device that uses materials that do not match the given default values of the ATLAS software and the format for the material statement is as follows:

```
MATERIAL <localization><material_definition>
```

Different parameters can be defined with different material statements. Examples include the bandgap at room temperature (EG300), electron and hole mobilities (MUN and MUP), recombination parameters (TAUN and TAUP), etc.

In our example, we used Graphene and MoS_2 and Si as basic materials in building the structure. The following statements are used to define their properties.

```
Material material=Graphene user.group=semiconductor
/user.default=4H-SIC

Material material=Graphene EG300=0.026 NC300=1.9e16 /
NV300=1.9e16 MUN=16983.69 MUP=16983.69

Material material=MoS2 user.group=semiconductor
/user.default=MoSi2

Material material=MoS2 EG300=1.29 NC300=2.2e18 /
NV300=1.8e19 MUN=100 MUP=150
```

As a user-defined material, it is necessary to identify to which material group Graphene does belong. Therefore, for its material definition statement, we specified that Graphene does belong to the “semiconductor” material group, using Silicon Carbide (4H-SiC) as a reference material, to be able to alter its properties and transform it to Graphene [81].

For MoS_2, its material definition statement, we specified that MoS_2 does belong to the “semiconductor” material group, using $MoSi_2$ as a reference material, to be able to alter its properties and transform it to MoS_2 .

4.3.2 MODELS

The physical models fall into five categories: mobility, recombination, carrier statistics, impact-ionization, and tunneling. The syntax of the model statement is as follows:

```
MODELS <model flag><general_parameter> / <model_dependent_parameters>
```

The choice of model depends on the materials chosen for simulation. The example below activates several models.

```
MODELS CONMOB FLDMOB SRH
```

CONMOB is the model for the concentration dependent mobility.

FLDMOB is the model of Dependence of the electric field.

SRH is the Shockley-Read-Hall model.

4.3.3 Contact

Contact determines the physical attributes of an electrode: anode, cathode, drain, etc. The syntax for contact is as follows:

```
CONTACT NUMBER=<n> |NAME=<name>|ALL
```

Here is our example of a contact statement:

```
contact name=anode workfunction=4.55
```

4.3.4 Numerical METHOD selection

After the materials model specification, the numerical method selection must be specified. Thereare various numerical methods to calculate solutions to semiconductor device problems. Thereare three types of solution techniques used in SILVACO ATLAS:

- Decoupled (GUMMEL)
- Fully coupled (NEWTON)
- BLOCK

The **GUMMEL** method solves for each unknown by keeping all other unknowns constant. The process is repeated until there is a stable solution. Newton's method solves all unknowns simultaneously. The **BLOCK** method solves some equations with the **GUMMEL** method and the others with the **NEWTON** method.

The **GUMMEL** method is used for a system of equations that are weakly coupled and where there is linear convergence. **NEWTON** method is used when the equations are strongly coupled with quadratic convergence. In our example, we used the following **Method** order

```
METHOD GUMMEL NEWTON BLOCK
```

In this example, equations are resolved by a GUMMEL method. If the convergence cannot be reached then NEWTON helped solve some of the equations and the others were solved by BLOCK. Solutions Specification

So far, we have created the structure, allocated the materials to their specific regions, gave them their properties, specified the physical models, and selected the numerical method for the calculations to be done. The next step is to specify solutions.

To evaluate a solar cell created in DECKBUILD or any other structure defining program, the user can simulate the actual conditions in which a solar cell would operate. This includes variables such as a light beam with its associated optical intensity and angle of incidence, different voltage conditions on the electrodes, and temperatures, to then extract and study the important optical-electrical parameters such as:

- The Current-Voltage curve (I-V curve)
- The Short Circuit Current (I_{sc})
- The Open Circuit Voltage (V_{oc})
- The Fill Factor
- The Efficiency η (%)

4.4 Solutions Specification

4.4.1 Defining the light source

In simulating solar cells, the user must specify a **beam of light**, which shines upon the device, and can then use any number of electrode conditions and solve statements to gather the desired characteristics of our Graphene/GaAs solar cell.

In this work, the light beam and the electrodes are utilized to set the environment for obtaining solutions of solar cell simulations.

BEAM: In DECKBUILD, the BEAM statement, which is used in obtaining solar cell solutions, comes after all of the structure defining statements and before the following solve statements. The light beam defining statement in this work is the following:

```
Beam num=1 x.o=10 y.o=-1 AM1.5
```

In this statement, we specified a light beam of AM1.5 spectral irradiance and the origin of the light beam that is located 1 μm above the center of our Graphene/GaAs solar cell.

4.4.2 Obtaining solutions

Before inputting statements that obtain all of the pertinent solutions for a device, files must be created to store all of the following solutions. These files can be of two types: **.log** and **.str** (structure) files.

LOG: allows all final simulation characteristics to be saved in a .log file (saves a file of .log extension). Any type of data, whether I-V, transient or C-V, generated by the `SOLVE` command is saved after the `LOG` command (thus the saved information is of the electrical type and is, for example, dependent on the

voltage Polarization or light source). If in the program there are several `LOG` commands, each time the log file that was opened before is closed, and a new log file is opened.

The following shows an example of the `LOG` statement.

```
LOG outfile=myoutputfile.log
```

The example saves the current-voltage information into myoutputfile.log, whichcan be viewed graphically in Tonyplot, which allows the user to specify the specific parts of the solution to a graph, as many solutions are all contained in one file and cannot be graphed simultaneously.

Structure files can be saved after a specific solve statement. This file stores all of the data from the solution and allows it to be viewed visually on the device structure. An example of the resulting structure file following a solve statement is given in Figure 23. Tonyplot can convert the numerical data saved into the structure file into a visual representation within the device. Photogeneration rates in the solar cell were stored into the structure file in shown in Figure 4-11. Red and orange regions represent higher photogeneration rates while yellow regions show the lowest photogeneration rates.

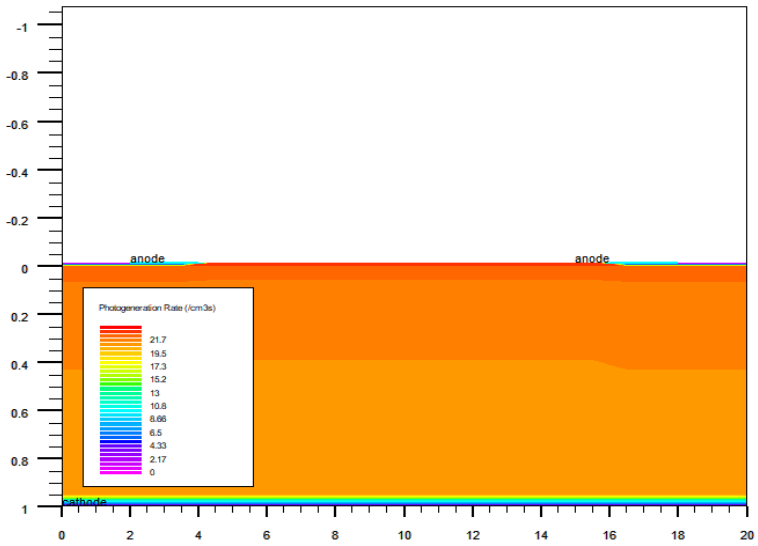

Figure 4-11:Photogeneration data is displayed in different areas of the solar cell.

After defining a log file in which all solutions are to be stored, ATLAS software does an initial solving of the doping profile and the potential at every mesh point in the zero-electrode bias case. This initial solution is obtained when there is no initial reference zero bias solution but can be specified by the statement solve init. After this initial solve statement, the conditions for the specific solve statements can be set. In simulating the operation of a solar cell.

SOLVE: The `SOLVE` statement follows the `LOG` statement. `SOLVE` performs a solution for one or more bias points. The following `SOLVE` statement is the one that was used in our study to obtain the solutions.

```
SOLVE b1=1.0
```

This statement applies the equivalent of **one sun** from the earlier defined light source (in BEAM statement) and solves the pertinent quantities, such as photogeneration rates and optical intensities, at each mesh point as well as the electrode currents.

After the beam of light has been applied, solutions at different electrode voltages can be obtained to create the solar cell's I-V curve.

```
solve vanode=0 name=anode vstep=0.1 vfinal=0.7
```

This statement is to obtain solutions for the illuminated solar cell at a range of anode voltages. It declares an initial anode voltage of 0 V and obtains solutions in the range from 0 V to 0.7 V in increments of 0.1 V.

By sweeping across anode voltages from 0 V to V_{oc} for the solar cell, the I-V curve is obtained. The results can later be displayed in Tonyplot in the form of a graph.

LOAD AND SAVE: The LOAD statement enters previous solutions from files as initial guess to other bias points. The SAVE statement enters all node point information into an output file.
The following are examples of LOAD and SAVE statements:

```
save outf= MoS2_01.str
```

In this case, `MoS2_01.str` has information saved after a `SOLVE` statement. Then, in a different simulation, `MoS2_01.str` can be loaded as follows:

```
Load infile= MoS2_01.str
```

4.5 Results' Analysis

Once a solution has been found for a semiconductor device problem, the information can be displayed graphically with TonyPlot. Additionally, device parameters can be extracted with the `EXTRACT` statement, which can be written manually in DECKBUILD, or selected from the "Insert Extract" menu from the "Commands" button in DECKBUILD's menu bar.

In the example below, the `EXTRACT` statement obtains the current and voltage characteristics of a solar cell. This information is saved into the `IVcurve.dat` file, then, TonyPlot displays the information in the IVcurve.dat file in the form of a graph.

```
      EXTRACT     NAME="iv"     curve(v."anode",i."cathode")     /
OUTFILE="IVcurve.dat"
      TONYPLOT IVcurve.dat
```

The following figure is an example of a solar cell's I-V curve displayed in Tonyplot using a simulation script of a silicon solar cell, which came pre-installed with SILVACO (TCAD).

IV.II SIMULATION RESULTS AND DISCUSSION

1. INTRODUCTION

In this chapter, we are going to talk about the results that we have gathered from the simulation. the add of thin film of MoS_2 applid are applied to observe their effect on the value of Efficiency, Fill Factor, V_{oc} and J_{sc}. The results are then compared with the results from article Ref.01.

The structure was obtained easily, but the results couldn't be obtained due to the fact that many parameters were not mentioned in the article including:

- The densities of state (N_C and N_V)
- The recombination parameters
- The Dielectric permittivity of Graphene and MoS_2
- The optical parameters, including the refractive index that was used to obtain the optical transmittance of Graphene and MoS_2

Efforts were put to obtain these parameters, through calculations and research.

2. GRAPHENE AND MoS_2 PARAMETERS OBTAINED AND USED IN THIS WORK

Silicon Carbide (4H-SiC) was used as a base material for modeling graphene and the Molybdenum silicide was used as a base material for modeling MoS_2.

and we have to determine the value we use in this work summarized in the following table:

Table 4-1. The parameters of graphene [82-85]. and MoS_2 [86] that were used in the simulation

Parameter type	ATLAS Identifier	Value for graphene	Value for MoS_2
Band parameters	Bandgap (E_g)	0.026	1.29
	Permittivity (ε)	5.6	4.17
	Work function	4.8	4
	Effective density of states in conducsion band	1.9e16	2.2e+18
	Effective density of states in valance band	1.9e16	1.8e+19
	Hole band mobility	16983.69	150
	Eletrone band mobility	16983.69	100
	Electrone affinity	4.08	4.2
Recombination parameters	taun0,taup0	0	0
	nsrhn,nsrhp	0	0
	ksrhcn,ksrhcp	0	0
	ksrhtn,ksrhtp	0	0
	ksrhgn,ksrhgp	0	0
	augn,augp	0	0
	augkn,augkp	0	0
	kaugcn,kaugcp	0	0
	kaugdn,kaugdp	0	0
	Etrap	0	0
	Copt	0	0

2.1 Refractive Index

One of the important optical parameters is the Refractive Index. It is to determine how much light is bent, or refracted, when entering a material. It is described by Snell's law of refraction:

$$n_1 \sin\theta_1 = n_2 \sin\theta_2 \tag{4.6}$$

Where θ_1 and θ_2 are the angles of incidence and refraction, respectively, of a light beam crossing the interface between two media with refractive indices n_1 and n_2.

The refractive indices also determine the amount of light that is reflected when reaching the interface, as well as the critical angle for total internal reflection and Brewster's angle.

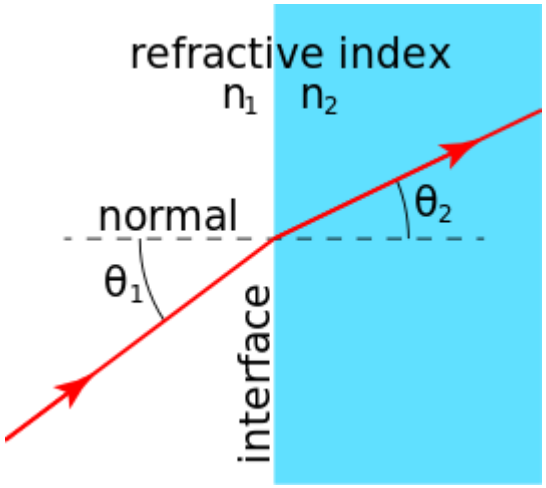

Figure 4-12: The refraction of a red-light beam traveling between two materials with different refractive indices.

2.1.1 Complex refractive index

When light passes through a medium, some part of it will always be attenuated (absorbed). This can be conveniently taken into account by defining a complex refractive index,

$$\underline{n} = n + i\kappa \tag{4.7}$$

Here, the real part n is the refractive index and indicates the phase velocity, while the imaginary part κ is called the extinction coefficient — although κ can also refer to the mass attenuation coefficient and indicates the

amount of attenuation when the electromagnetic wave propagates through the material.

In the case of graphene, a small part of the light passing through it is attenuated. Thus, it's refractive index is represented in a complex from.

It is important to know that, unlike other studies, the values of graphene's refractive index that were introduced in this work are **Wavelength dependent,** which gives us the following relation of graphene's refractive index

$$\underline{n}(\lambda) = n(\lambda) + i\kappa(\lambda) \tag{4.8}$$

The two following graphs represent the values of graphene's and MoS_2 refractive index depending on the optical wavelength:

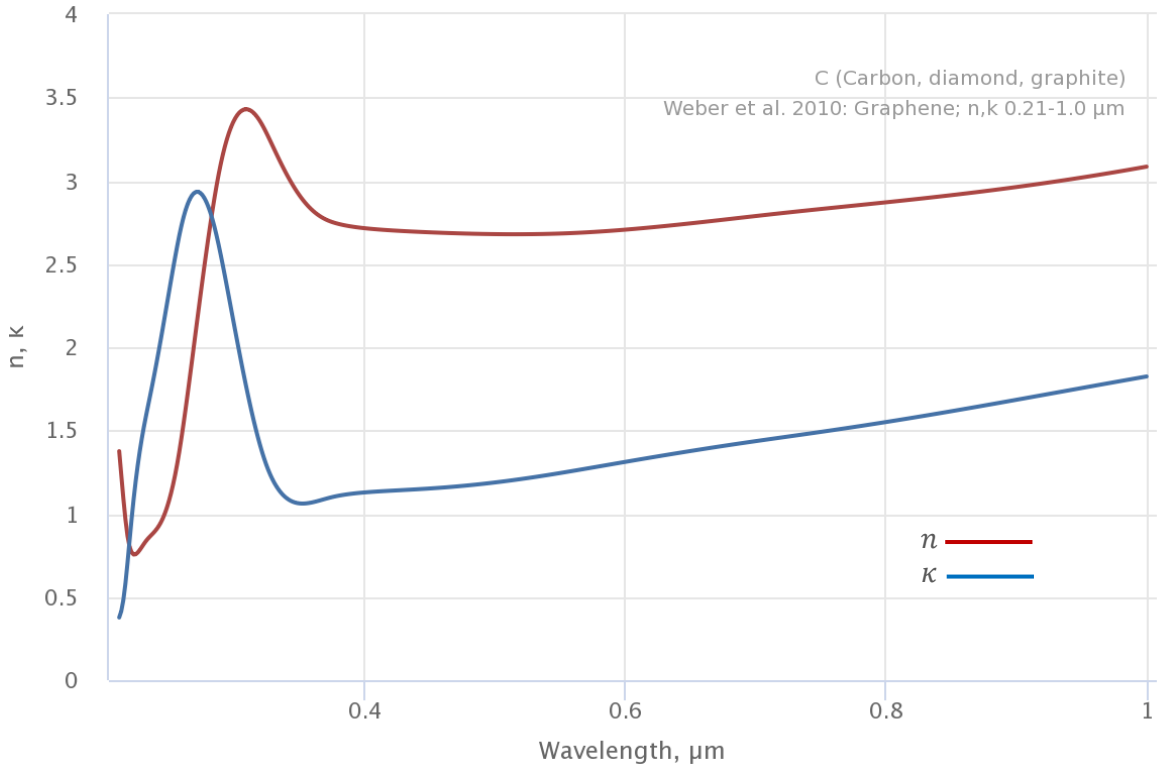

Figure 4 -13: Real and Imaginary refractive index of graphene versus Optical Wavelength [87].

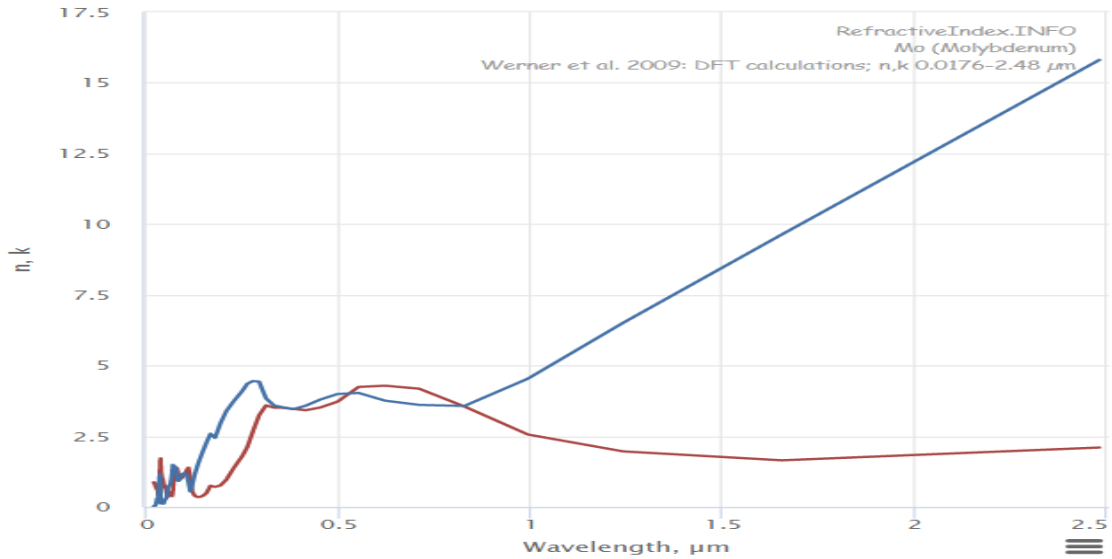

Figure 4 -14: Real and Imaginary refractive index of MoS_2 versus Optical Wavelength[88].

These values were used in our simulation, which allowed us to obtain results that are close to the experimental values published in reference [01]

3. RESULTS AND DISCUSSION

3.1 Results:

In this worck, we study and compare two different Schottcky solar cells; the first one is graphene/n-Si and the second one is Graphene/MoS2/n-Si. Table 4-2 summarizes the results obtained in this work.

Table 4-2: Results of the simulation

Solar cells type	V_{oc}(V)	J_{sc}(mA/cm^2)	Format Factory	Efficiency %
Graphene/n-Si	0.62	6.9	0.87	2.7
Graphene/MoS_2/n-Si	0.425	0.66	22.2	4.5

3.1.1 The following graphs confirm the diode behavior of our structures

Dark graph:

Graphene/Si

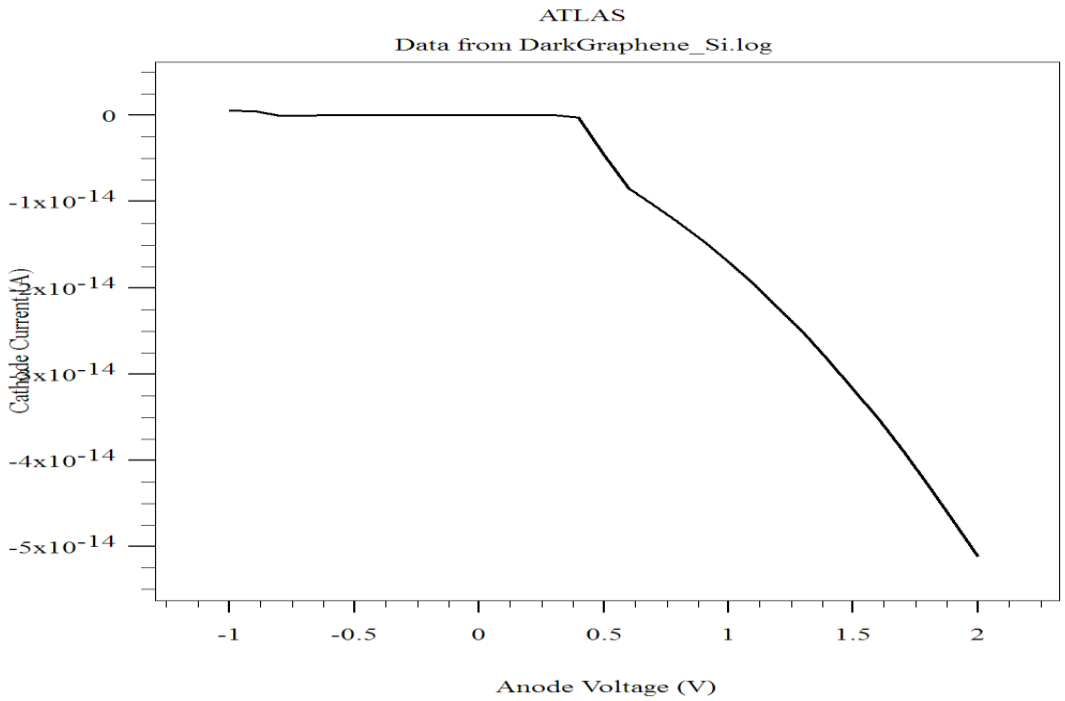

Figure 4 -15: Graphene/Si in Dark Mode

Graphene/MoS2/Si

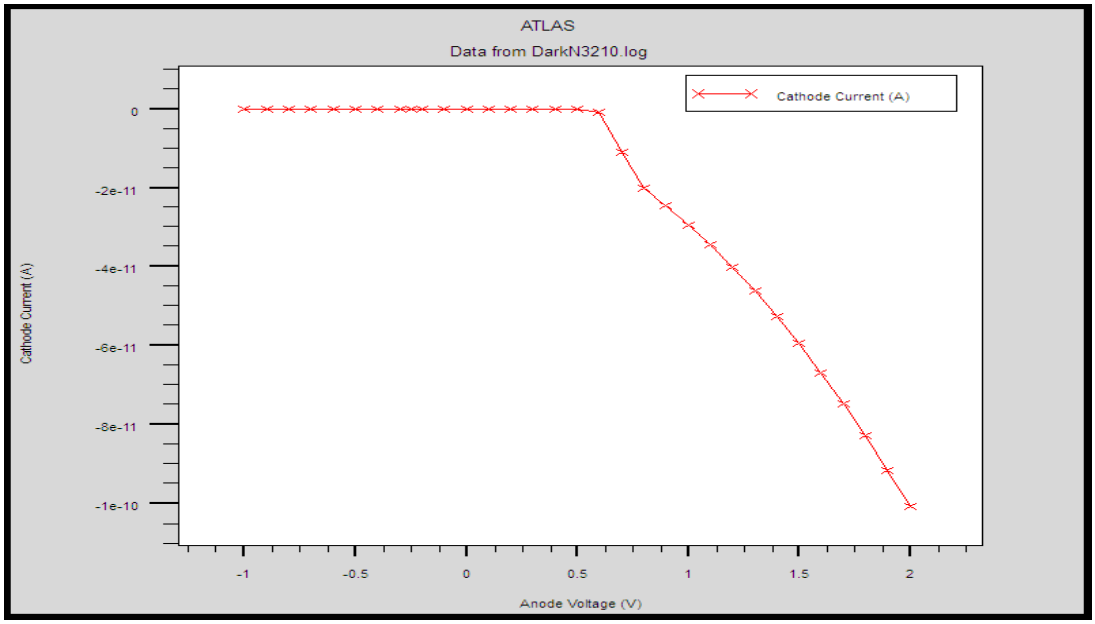

Figure 4 -16: Graphene/MoSi/Si in Dark Mode

Light Graph:

Graphene/Si

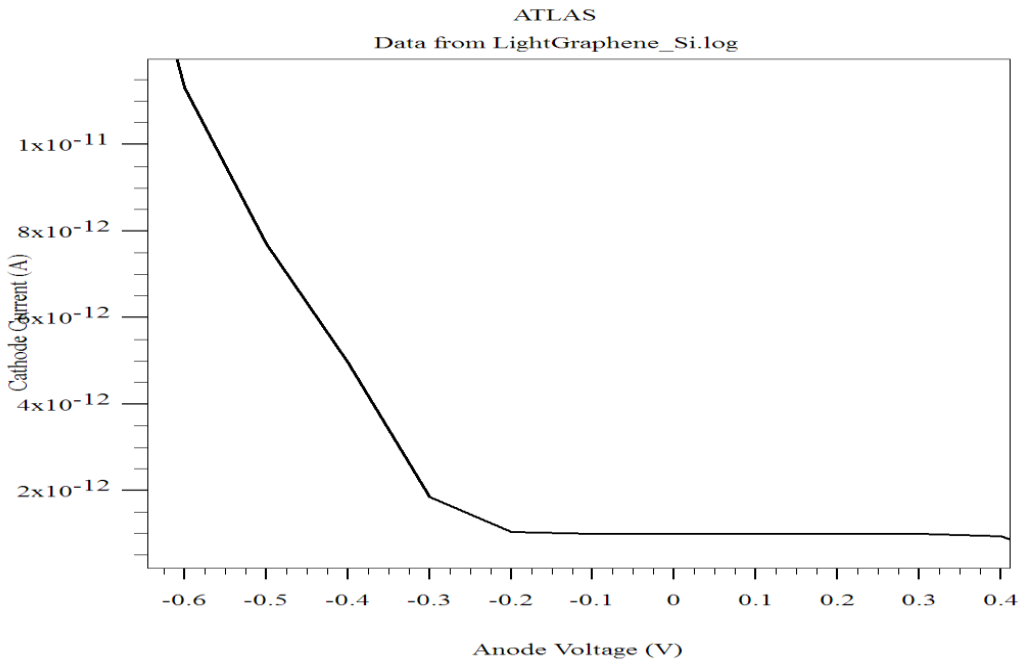

Figure 4 -17: Graphene/Si in Light Mode

Graphene/MoS2/Si

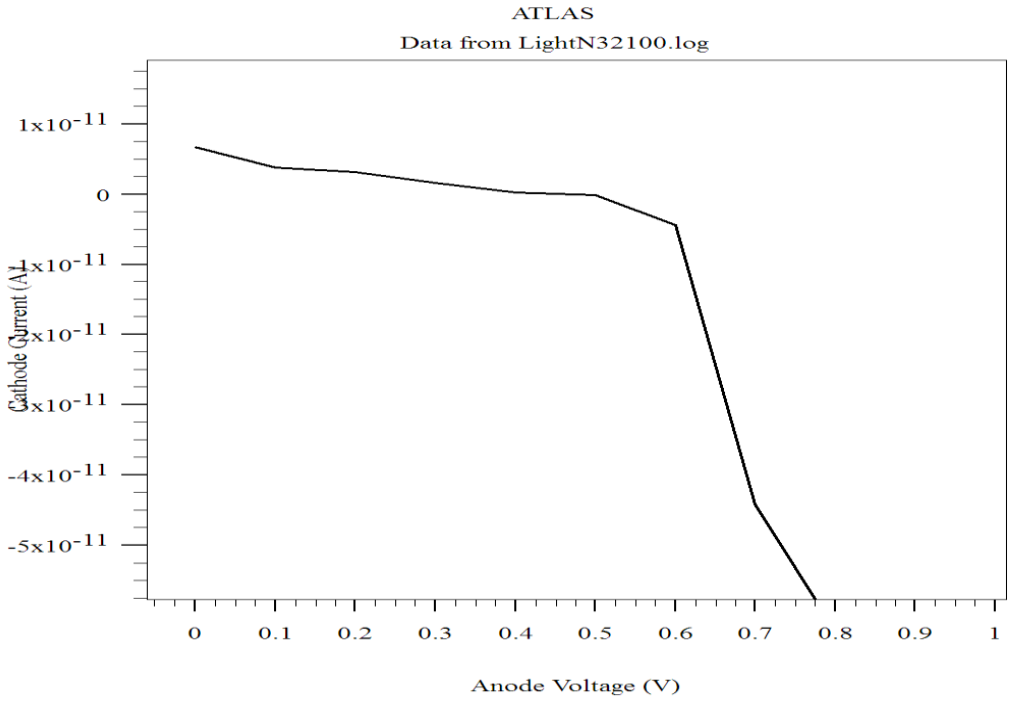

Figure 4 -18: Graphene/Si in Light Mode

3.1.2 Observation :

We observe that there is an increase in the efficiency of the solar cell when we insert a thin film of MoS_2 of almost we double value.

3.1.3 MoS_2 effect:

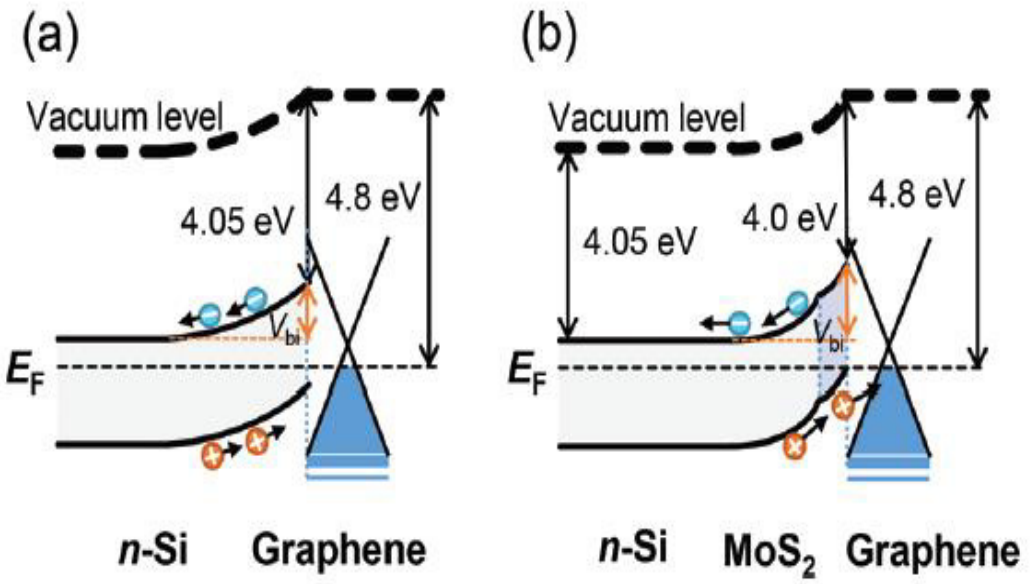

Figure 4-19: Schematics of band diagrams for the solar cells [1].

To better understand the photovoltaic process, we show band alignment diagrams for the graphene/n-Si and graphene/MoS_2/n-Si solar cells, as shown in Fig. 4-15(a) shows the band alignment of a graphene/n-Si solar cell under ambient conditions. The photovoltaic process in the graphene/n-Si solar cells is understood by the Schottky barrier formed at the semimetal (graphene) and semiconductor (n-Si) interface. Fig. 4-15(b) shows a schematic band diagram for graphene/ MoS_2/n-Si solar cells. We confirmed that thin film MoS_2 exhibits n-type properties [1]. The total built-in voltage (Vbi) of graphene/MoS_2/n-Si solar cells is greater than that of the graphene/ n-Si solar cell because the Schottky barrier height is determined by the energy difference between the electron affinity χs of the semiconductor and the work function Wm ofgraphene, i.e. Wm − χs.The increase of the built-in field by insertion of an MoS_2 layer can directly improve the VOC and the photovoltaic conversion efficiency. Moreover, because of the difference between the Fermi levels, the bottom of the conduction band and the top of the valence band of the MoS_2 layer at the interface of graphene are shifted upward, resulting in an energy barrier at the interface between MoS_2 and n-Si. The energy barrier of the MoS_2 layer functions as an effective electron blocking layer for the photogenerated electrons in the Si layer. Furthermore, in the case of the photogenerated hole, the energy barrier created by the MoS_2 layer functions as an effective hole-transport layer. The effective carrier transporting (blocking) layer of MoS_2 effectively reduces the recombination loss of carriers, which in turn results in an increase of the JSC. Therefore, the MoS_2 layer between the graphene and n-Si contributes to the enhancement of photovoltaic performance as a carrier transporting (blocking) layer.

4. Chapter conclusion:

In this chapter, we presented the software that is used in our work to simulate a Graphene/n-Si and Graphene/MoS_2/n-Si solar cells. We showed the different steps to create the structure, allocate materials, give these materials their respective properties, study the optical-electrical behavior of our devices and extract the different important solar cell parameters.

These results showed us that the most important factors for higher efficiencies are the nano layer of MoS_2

Thus, the results provide a new opportunity to increase solar cells effecienc.

V. GENERAL CONCLUSION

In this work, we explained how a graphene/Si solar cell efficiency get increased by inserting a nano layer of MoS2 material using SILVACO ATLAS (TCAD). The unique properties of graphene and MoS_2 layers on the surface of the silicon substrate allow for a better charge holder because of the ease of transport of electrons and low recombination rates, with very small losses in light input energy based on the two-dimensional layer of light transmission. We also validate the experiemental work of reference [1]. First, we validated that the efficieny get increased by inserting the Nano layer of MoS2. In addition, we verified that the efficiency decreased with incresed thickness of MoS2.

We investigated the considerable improvement in the photovoltaic performance of graphene/Si solar cells using MoS_2. MoS_2 acts as effective layer of hole transport / electron blocking. This property contributes remarkably in improving the efficiency of graphene / MoS_2 / n-Si solar cell.

in principal the effective transport (blocking) layer of the carrier in MoS_2 reduces the recombination loss of the carriers, which in turn leads to an increase in JSC. Therefore, the MoS_2 layer between graphene and n-Si enhances the photoelectric performance as a carrier (blocking) carrier layer, it gives us an increase in efficincey.

The performance of our solar cell is highly dependent on graphene-based Schottky and MoS_2 connection properties. Superior mobility allows shippers to better collect current, allowing them to travel by connecting to a low resistance path.

Solar cells are currently considered a high priority in human life as a viable source of renewable energy and as a source of energy in remote areas such as space or the countryside. We recommend intensifying research on improving the efficiency of solar cells in our universities and research centers, where countries are switching from traditional sources of energy, such as fossil fuels, by attempting to make good use of solar cells for more energy from

renewable resources for domestic and industrial use, allowing the convergence and delivery of technologies and facilitating human life In particular.

LIST OF SYMBOLS

Symbol	Name	Unit
h	Planck's constant	$eV.s$
ν	Photon frequency	s^{-1}
c	Light speed in vacuum	m/s
K_B	Boltzmann constant	$photons.cm^{-2}s^{-1}$
T	Room temperature	$°K$
q	Elementary charge	C
W	Depletion region width	μm
λ	Photon Wavelength	μm
N_C, N_V	Densities of State	cm^{-3}
E_F	Fermi energy state level	eV
E_C	Lowest level of energy in the conduction band	eV
E_V	Lowest level of energy in the valence band	eV
n_i	Intrinsic concentration	cm^{-3}
n	Density of free electrons	cm^{-3}
p	Density of free holes	cm^{-3}
ϕ_B	Schottky Barrier height	eV
ϕ_m	Metal work function	eV
χ	Electron affinity in a semiconductor	eV
V_{BI}	Built-in potential	eV
ϕ_s	Semiconductor work function	eV
N_a , N_d	Concentration of acceptors and donors respectively	cm^{-3}
V_{OC}	Open circuit voltage	V
V_A	Applied voltage	V
V_{max}	Maximum power voltage	V
I_{SC}	Short circuit current	mA
I_F	Forward bias current	mA
I_{max}	Maximum power current	mA
I_0	Initial current	mA
I_R	Reverse bias current	mA
k	Boltzmann's constant	$eV.K^{-1}$
A	Area of contact between metal and semiconductor	cm^2
R_S	Series resistance	Ω
V_{RB}	Reverse Bias Voltage	V
ε_m	Permittivity in metal	$F \cdot cm^{-1}$
ε_0	Permittivity in vacuum	$F \cdot cm^{-1}$
P_{max}	Maximum power	$Watts$
FF	Fill Factor	%
η	Efficiency	%
$A.M$	Air mass	
E	Photon energy	eV
E_g	Energy Bandgap	eV
MoS_2	molybdenum disulfide	

$MoSi_2$	*molybdenum silicide*	
Si	*Silicon*	
$4H-SiC$	*Silicon carbide*	
τ_c	*Mean free time between collisions*	s
$\underline{n}$	*Complex refractive index*	
n	*Real part of the complex refractive index*	
κ	*Imaginary part of the complex refractive index*	
R_{SH}	*Sheet resistance*	Ω/sq
ρ	*Resistivity*	$\Omega.cm$
μ_n, μ_p	*Electron and hole mobilities*	$cm^2/V.s$
t	*Graphene thickness*	nm

REFERENCES:

[01] Enhanced photovoltaic performances of graphene/Si solar cells by insertion of a MoS_2 thin film, Yuka Tsuboi,a Feijiu Wang,a Daichi Kozawa, March 2015

[02] A. K. Geim and K. S. Novoselov, The Rise of Graphene, Nat. Mater., 2007, 6, 183–191.

[03] A. Splendiani, L. Sun, Y. Zhang, T. Li, J. Kim, C.-Y. Chim, G. Galli and F. Wang, Emerging Photoluminescence in Monolayer MoS_2, Nano Lett., 2010, 10, 1271–1275.

[04] B. Radisavljevic, A. Radenovic, J. Brivio, V. Giacometti and A. Kis, Single-layer MoS_2 Transistors, Nat. Nanotechnol., 2011, 6, 147–150.

[05] C. N. R. Rao, A. K. Sood, K. S. Subrahmanyam and A. Govindaraj, Graphen, Das Neue Zweidimensionale Nano- material, Angew. Chem., Int. Ed., 2009, 121, 7890–7916.

[06] Z. He, Y. Sheng, Y. Rong, G.-D. Lee, J. Li and J. H. Warner, Layer-Dependent Modulation of Tungsten Disulfide Photo- luminescence by Lateral Electric Fields, ACS Nano, 2015, 9, 2740–2748.

[07] Y. Saito and Y. Iwasa, Ambipolar Insulator-to-Metal Tran- sition in Black Phosphorus by Ionic-Liquid Gating, ACS Nano, 2015, 9, 3192–3198.

[08] S. Li, Y. Luo, W. Lv, W. Yu, S. Wu, P. Hou, Q. Yang, Q. Meng, C. Liu and H. M. Cheng, Vertically Aligned Carbon Nanotubes Grown on Graphene Paper as Electrodes in Lithium-Ion Batteries and Dye-Sensitized Solar Cells, Adv. Energy Mater., 2011, 1, 486–490.

[09] D.-M. Sun, M. Y. Timmermans, Y. Tian, A. G. Nasibulin, E. I. Kauppinen, S. Kishimoto, T. Mizutani and Y. Ohno, Flexible High-Performance Carbon Nanotube Integrated Circuits, Nat. Nanotechnol., 2011, 6, 156–161.

[10] Novoselov, K. S. et al. Electric field effect in atomically thin carbon films. Science 306, 666–669 (2004).

[11] M. Burghard, H. Klauk, and K. Kern, Adv. Mater. 21, 2586 (2009).

[12] X. Li, Y. Zhu, W. Cai, M. Boryslak, B. Han, D. Chen, R. D. Piner, L. Colombo, and R. S. Ruoff, Nano Lett. 9, 4359 (2009).

[13] H. G. Craighead, J. Cheng, and S. Hackwood, Appl. Phys. Lett. 40, 22 (1982). 5. S. R. C. Vivekchand, C. S. Rout, K. S. Subrahmanyam, A. Govindaraj, and C. N. R. Rao, J. Chem. Sci. 120, 9 (2008).

[14] D. A. Dikin, S. Stankovich, E. J. Zimney, R. D. Piner, G. H. B. Dommett, G. Evmenenko, S. T. Nguyen, and R. S. Ruoff, Nature 448, 457 (2007).

[15] F. Schedin, A. K. Geim, S. V. Morozov, E. W. Hill, P. Blake, M. I. Katsnelson, and K. S. Novoselov, Nat. Mater. 6, 652 (2007).

[16] G. Wang, X. Shen, J. Yao, and J. Park, Carbon 47, 2049 (2009).

[17] J. Li, J. Chen, B. Shen, X. Yan, and Q. Xue, Appl. Phys. Lett. 99, 163103 (2011).

[18] D. Ye, S. Moussa, J. D. Ferguson, A. A. Baski, and M. S. Shall, Nano Lett. 12, 1265 (2012).

[19] X. Li, H. Zhu, K. Wang, A. Cao, J. Wei, C. Li, Y. Jia, Z. Li, X. Li, and D. Wu, Adv. Mater. 22, 2743 (2010).

[20] W. J. Hong, Y. X. Xu, G. W. Lu, C. Li, and G. Q. Shi, Electrochem. Commun. 10, 1555 (2008).

[21] J. A. Wilson and A. D. Yoffe, The Transition Metal Dichalco- genides Discussion and Interpretation of the Observed Optical, Electrical and Structural Properties, Adv. Phys., 1969, 18, 193–335.

[22] K. F. Mak, C. Lee, J. Hone, J. Shan and T. F. Heinz, Atomic- ally Thin MoS_2: A New Direct-Gap Semiconductor, Phys. Rev. Lett., 2010, 105, 136805.

[23] L. Chu, H. Schmidt, J. Pu, S. Wang, B. Özyilmaz, T. Takenobu and G. Eda, Charge Transport in Ion-Gated Mono-, Bi-, and Trilayer MoS_2 Field Effect Transistors, Sci. Rep., 2014, 4, 7293.

[24] J. Guo, “Carbon Nanotube Electronics, Modeling, Physics, and Applications,” Doctoral Dissertation, Purdue University, 2004.

[25] B. Zeghbroeck, Principles of Electronic Devices, http://ecee.colorado.edu (accessed March 4, 2012).

[26] A. Bates, “Novel Optimization Techniques for Multijunction Solar Cell Design USING SILVACO ATLAS,” Master’s Thesis, Naval Postgraduate School, 2004.

[27] Metal Semiconductor Junctions” Retrived: June 1, 2007 Copyright 2004 B. Van Zeghbroeck http://ece www.colorado.edu/~bart/book/book/chapter3/ch3_3.htm

[28] Ben G Streetman “Solid State Electronic Devices” 3rd Edition, Prentice Hall Series in Solid State Physical Electronics. ISBN 0-13-822941-4 Date: pg. 200 -205 December 1990.

[29] S. Michael, EC3230 Lecture Notes, Naval Postgraduate School, Winter 2004 (unpublished).

[30] S. Michael, “The Design and Optimization of Advanced Multijunction SolarCells,” Presented at the 35th IEEE PV Specialists Conference, Vancouver, Canada, 2004.

[31] Gueymard, C.; Myers, D.; Emery, K. (2002). "Proposed reference irradiance spectra for solar energy systems testing". Solar Energy. 73 (6): 443–467. doi:10.1016/S0038-092X(03)00005-7.

[32] Reference Solar Spectral Irradiance & PV Cell Operational Regions (ASTM G173-03) ASTM

[33] C.BALLIF, Electrics and Optics of WS2 and MoS_2 Couches and Photovoltaic Applications, The Doctorate, ÉCOLE POLYTECHNIQUE FÉDÉRALE DE LAUSANNE, 1998.

[34] Molybdenum product du jour-SCF.www.societechimiquedefrance.fr

[35] https://en.wikipedia.org/wiki/Molybdenum_disulfide

[36] Stefan Seegerm, Fabrication and Characterization of the Lattice Sulfide MoS_2 and WS2 for Photovoltaic Applications, Grades Doktor, Berlin, 2006.

[37] Crystallography Reviews Review of material properties of (Mo / W) Se2-layered compound semiconductors useful for photoelectrochemical solar cells, S. Mary Delphine, M. Jayachandran, C. Sanjeeviraja, 2014.

[38] Mingxiao Ye, Dustin Winslow, Dongyan Zhang, Ravindra Pandey and Yoke Khin Yap Recent Advancement on the Optical Properties of Two-Dimensional Molybdenum Disulfide (MoS_2) Thin Films, Department of Physics, Michigan Technological University, 1400 Townsend Drive, Houghton, MI 49931, USA; 2015.

[39] Preparation and grouth of materials with layred structure, ed. R.M.A. Lieth, D.Reidel, Dordrech, The Netherlands, 1977, vol.1.

[40] C. ZIMEI, Preparation of oriented Molybdenum disulfide thin film for photoelectrochemical energy harvesting applicationsm, for the degree of master of science, university of SINGAPORE, 2014.

[41] Seminar II, Scanning tunneling spectroscopy of flat and curved MoS_2 crystals, Author: Stefan Krek, Mentor: doc. Maja Rem˘skar, 25th March 2008, University of Ljubljana Faculty of Mathematics and Physics Department of Physics.

[42] Emerging Energy Applications of Two-Dimensional Layered Materials, Dattatray J. Late, Chandra Sekhar Rout, Disha Chakravarty and Satyajit Ratham, Canadian Chemical Transactions, 2015.

[43] Qing Hua Wang, Kourosh Kalantar-Zadeh, Andras Kis, Jonathan N. Coleman and Michael S. Strano, Electronics and optoelectronics of two-dimensional transition metal dichalcogenidesm, NATURE NANOTECHNOLOGY | VOL 7 | NOVEMBER 2012

[44] D.Dophil, Synthesis and Characterization of Nanoparticles and Fullerens of Dichalcogenes of Transition MX2 (où M = Mo, W; X = S, Se), Université de paris XII-VALDEMARNE, 2003.

[45] Proprietary optics and the transport of monos couches of MoS_2 and discs associates, Xavier MARIE (Laboratory of Physics and Chemistry of Nano-Objects), ANR L'Agence national de la recherche Des projects for science, 2014.

[46] S .MEZIANE, Ab initio study of transition metal chalcogenides IVBX2 or VBX2 (X = S, Se or Te), University ABOU BEKR BELKAID - TLEMCEN, 2014.

[47] L. J.-POTTUZ, Lubricating nanoparticles with closed structure, doctoral thesis, the central school of LYON, 2005.

[48] J.Chang, Leonard F. Register and Sanjay K. Banerjee Comparison of Ballistic Transport Characteristics of Monolayer Metal Transition Dichalcogenides (TMDs) MX2 (M = Mo, W; X = S, Se, Te) n-MOSFETs, The University of Texas at Austin, 2013 IEEE.

[49] L.CHIBANE, Study of the electrical and structural properties of the semiconductor lamellar MoS_2 for a photovoltaic application, thesis of magister, UMMTO, 2009.

[50] Novoselov, K. S. et al. Electric field effect in atomic thin carbon films. Science 306, 666 (2004).

[51] Landau, L. D. Zur theorie der phasenumwandlungen II. Phys. Z. Sowjetunion 11, 26 (1937).

[52] http://evworld.com/article.cfm?storyid=1950.

[53] Bae, S. et al. Towards industrial applications of graphene electrodes. Physica Scripta 2012, 014024 (2012).

[54] Nika, D. L. & Balandin, A. A. Two-dimensional phonon transport in graphene. J. Phys. Condens. Matter 24, 233203 (2012).

[55] Saito, R., Dresselhaus, G. and Dresselhaus, M. S. Physical properties of carbon nanotubes. Imperial College Press, London (1998).

[56] Castro Neto, A. H. et al. The electronic properties of graphene. Rev. Mod. Phys. 81, 109 (2009).

[57] Wong, H.-S. P. & Akinwande, D. Carbon Nanotube and Graphene Device Physics. Cambridge University Press (2011).

[58] Ando, T. The electronic properties of graphene and carbon nanotubes. NPG Asia Mater. 1, 17 (2009).

[59] Geim, A.K. & Novoselov, K. S. The rise of graphene. Science 6, 183 (2007).

[60] Lee, C. et al. Measurement of the elastic properties and intrinsic strength of monolayer graphene. Science 321, 385 (2008).

[61] Cai, D., Yusoh, K. & Song, M. The mechanical properties and morphology of a graphite oxide nanoplatelet / composite polyurethane. Nanotechnology 20, 085712 (2009).

[62] Bae, S. et al. Roll-to-roll production of 30-inch graphene films for transparent electrodese. Nature Nanotechnology 5, 574 (2010).

[63] Ryh¨anen, T. et al. Nanotechnologies for Future Mobile Devices. Cambridge University Press (2010).

[64] Nair, R. R. et al. Fluorographene: A two-dimensional counterpart of teflon. Small 6, 2877 (2010).

[65] http://www.graphene.manchester.ac.uk/story/image gallery /.

[66] Scarpa, F., Chowdhuryb, R. & Adhikarib, S. Thickness and in-plane elasticity of graphane. Physics Letters A 375, 2071 (2011).

[67] http://cnx.org/content/m29187/latest/.

[68] Elias, D.C. et al. Control of graphene's properties by reversible hydrogenation: Evidence for graphane. Science 323, 610 (2009).

[69] Dikin, D.A. et al. Preparation and characterization of graphene oxide paper. Nature 448, 457 (2007).

[70] Bagri, A. et al. Structural evolution during the reduction of chemically derived graphene oxide. Nature Chemistry 2, 581 (2010).

[71] Gao, W. et al. New insights into the structure and reduction of graphite oxide. Nature Chemistry 1, 403 (2009).

[72] Nair, R. R. et al. Unimpeded permeation of water through helium-leak-tight graphene-based membranes. Science 335, 442 (2012).

[73] "Silvaco rollout includes mixed-signal simulation". EE Times. Cambridge, Massachusetts: AspenCore. 7 June 2004. Retrieved 29 August 2019.

[74] "Software Gifts". ASU.edu. Arizona State Univerisity, the School of Electrical, Computer & Energy Engineering.

[75] Santarini, Michael (9 January 2006). "Simucad spins out of Silvaco with eye toward IPO". Electronics Weekly. Surrey, England: Metropolis International Group. Archived from the original on 24 December 2012.

[76] "TAOS tapes out mixed signal IC using Silvaco's place and route and EDA tool flow" (Press release). Silvaco. 17 February 2012.

[77] "Silvaco Enters IP Market With Acquisition of IPextreme". Silvaco.com. Retrieved 30 August 2019.

[78] "Silvaco Group Acquires edXact for SPICE Simulation Speed-up". Silvaco.com. Retrieved 30 August 2019.

[79] "Silvaco to Acquire SoC Solutions". GlobeNewsWire.com. Retrieved 30 August 2019.

[80] Atlas User's Manual"Device Simulation Software", Silvaco, Inc.4701 Patrick Henry Drive, Bldg. 2. Santa Clara, CA 95054 (2016).

[81] J. Brunton, TCAD Analysis of Heating and Maximum Current Density in Carbon Nanofiber Interconnects Master's Thesis, Naval Postgraduate School, (2011).

[82] J. W. Weber, V. E. Calado, and M. C. M. van de Sanden, "Optical constants of grapheme measured by spectroscopic ellipsometry", Department of Applied Physics, Eindhoven University of Technology, P.O. Box 513, 5600 MB Eindhoven, The Netherlands. (2010).

[83] P. Avouris and M. Freitag, "Graphene photonics, plasmonics, and optoelectronics," IEEE Journal on Selected Topics in Quantum Electronics, vol. 20, no. 1, Article ID 6000112, (2014).

[84] Alina Cismaru, Mircea Dragoman and Adrian Dinescu, "Microwave And Millimeterwave Electrical Permittivity Of Graphene Monolayer", arXiv: 1309.0990. Condensed Matter. Mesoscale and Nanoscale Physics. (2013).

[85] T. Feng, D. Xie, Y. Lin et al., “Graphene based Schottky junction solar cells on patterned silicon-pillar-array substrate,” Applied Physics Letters, vol. 99, no. 23, Article ID 233505, (2011).

[86] H. RASHIDa , K. S. RAHMANb , M. I. HOSSAINb,c , N. TABET c , F. H. ALHARBIc, N. AMINa, b/August 2014 PROSPECTS OF MOLYBDENUM DISULFIDE (MoS_2) AS AN ALTERNATIVE ABSORBER LAYER MATERIAL IN THIN FILM SOLAR CELLS FROM NUMERICAL MODELING, August 2014

[87] https://refractiveindex.info/?shelf=main&book=C&page=Weber

[88] https://refractiveindex.info/?shelf=main&book=Mo&page=Werner-DFT

[89] J. Pu, Y. Yomogida, K.-K. Liu, L.-J. Li, Y. Iwasa and T. Takenobu, Highly Flexible MoS_2 Thin-Film Transistors with Ion Gel Dielectrics, Nano Lett., (2012).